Soft computing-based models for the prediction of masonry compressive strength

Panagiotis G. Asteris[1*], Paulo B. Lourenço[2], Mohsen Hajihassani[3], Chrissy-Elpida N. Adami[1], Minas E. Lemonis[1], Athanasia D. Skentou[1], Rui Marques[2], Hoang Nguyen[4], Hugo Rodrigues[5] and Humberto Varum[6]

[1] *Computational Mechanics Laboratory, School of Pedagogical and Technological Education, Heraklion, GR 14121, Athens, Greece*

[2] *Department of Civil Engineering, ISISE, University of Minho, Guimarães, Portugal*

[3] *Department of Mining Engineering, Faculty of Engineering, Urmia University, 5756151818 Urmia, Iran*

[4] *Department of Surface Mining, Mining Faculty, Hanoi University of Mining and Geology, 18 Vien st., Duc Thang ward, Bac Tu Liem dist., Hanoi, Vietnam*

[5] *RISCO, Department of Civil Engineering, University of Aveiro, Aveiro, Portugal*

[6] *CONSTRUCT-LESE, Faculty of Engineering of the University of Porto, Civil Engineering Department, Porto, Portugal*

[*] *Corresponding author, Professor, E-mail: asteris@aspete.gr; panagiotisasteris@gmail.com*

Abstract: Masonry is a building material that has been used in the last 10.000 years and remains competitive today for the building industry. The compressive strength of masonry is used in modern design not only for gravitational and lateral loading, but also for quality control of materials and execution. Given the large variations of geometry of units and joint thickness, materials and building practices, it is not feasible to test all possible combinations. Many researchers tried to provide relations to estimate the compressive strength of masonry from the constituents, which remains a challenge. Similarly, modern design codes provide lower bound solutions, which have been demonstrated to be weakly correlated to observed test results in many cases. The present paper adopts soft-computing techniques to address this problem and a dataset with 401 specimens is considered. The obtained results allow to identify the most relevant parameters affecting masonry compressive strength, areas in which more experimental research is needed and expressions providing better estimates when compared to formulas existing in codes or literature.

***Keywords*:** artificial neural networks; genetic programming; machine learning; masonry; metaheuristic algorithms; compressive strength

Notations

AC	dense aggregate concrete
ACC	autoclaved aerated concrete
ANN(s)	Artificial Neural Network(s)
B	brick
BCB	burnt clay brick
BPNN	Back Propagation Neural Network
C	calcarenite
CCB	compressed cement block
CEB	compressed earth block
CeU	ceramic unit
ClB	clay brick
Co	Competitive transfer function
CoB	concrete block
CSB	calcium silicate block
CSEB	cement stabilized earth block
f_{bc}	compressive strength of the masonry unit [in MPa]
f_{mc}	compressive strength of the mortar [in MPa]
FS	flagstone
f_{wc}	compressive strength of wall or prism [in MPa]
GP	Genetic Programming
GS	granite stone
HCB	hollow concrete block
HCSB	hollow calcium silicate block
HHClB	horizontal hollow clay brick
HLC	hollow lightweight concrete
HTS	Hyperbolic Tangent Sigmoid transfer function
h_w	height of the wall or prism-to-thickness ratio
k	volume of mortar-to-volume of wall ratio
k_h	factor that accounts for the ratio of unit height to mortar joint thickness
k_m	code that accounts for the type of unit, the mortar compressive strength and the bedding type
k_o	ratio depending on the type of masonry (brick or stone masonry)
Li	Linear transfer function
LS	Log-Sigmoid transfer function
MAPE	Mean Absolute Percentage Error
MB	mud brick
MCU	modular cored unit
MSE	Mean Square Error
NDT	Non-Destructive Test
NRB	Normalized Radial Basis transfer function
OS	Ohio stone
PClB	perforated clay block
PCoB	perforated concrete block
PLi	Positive Linear transfer function

R	Pearson correlation coefficient
RB	Radial Basis transfer function
SBClB	solid burnt clay brick
SClB	solid clay brick
SCoB	solid concrete block
SCWB	soft clay wire-cut brick
SM	Soft Max transfer function
SMB	stabilized mud brick
SMP	standard modular paver
SSE	Sum Square Error
SSL	Symmetric Saturating Linear transfer function
TB	Triangular Basis transfer function
t_b	mean value of the masonry unit height
t_m	mean value of bed joint thickness
TMB	table mould brick
t_w	thickness of the wall or prism
v_m	relative volume of mortar
V_m	volume of mortar
VSCB	solid clay brick
v_u	relative volume of unit
V_{wall}	volume of wall
WB	wire-cut brick
α	factor that accounts the effect of the type and the shape of the masonry unit
α, b, c, m, n	constants for the analytical/empirical determination of the compressive strength of masonry
β	factor that expresses the effect of the interfacial transition zone and bond strength between the masonry unit and the mortar
K	constant depending on the material and on the group of the masonry unit, and the type of the mortar
ξ	factor that considers the influence of the thickness of the joints and the volume fraction of the mortar

1. Introduction

Masonry is a construction bearing system made from individual masonry units that are laid together with or without mortar. Masonry units may be either solid or hollow, and may be made of a wide variety of materials. The most common materials used as masonry units are adobe and clay brick, concrete block and natural stone block, whereas frequently used mortars consist of earth, aerial lime (with or without the addition of pozzolan), hydraulic lime or cement. The first evidence of Humanity using masonry building system (consisting from sundry bricks bonded with earth mortar) is placed back in 6500 BC (Engesser 1907, Khan and Lemmen 2013). Masonry construction is often preferred also in our days, not only in developing countries, due to its low cost compared to other modern materials, but also in developed countries, due to the aesthetic value, durability, solidity, fire resistance and other characteristics that it provides.

Masonry constructions are typically complex structures that require a thorough and detailed knowledge and information concerning the mechanical behaviour of their structural systems (Ceroni et. al. 2012). This is mainly related to the difficulty in estimating properties, composite and anisotropic nature of the material "masonry" (Syrmakezis and Asteris 2001, Lourenço 2002, Milani et al. 2006, Asteris et al. 2011, Chrysostomou, and Asteris 2012, Asteris et al. 2013, Asteris et al. 2014). Practice, as well as experimental testing, has shown that these structures have low resistance in tension and in shear, whereas their compressive strength is, in general, adequate for the level of loads of conventional structures. Actually, masonry buildings fail mainly due to diagonal cracking against in-plane actions or cracking with the formation of rotation lines against out-of-plane bending. Furthermore, masonry structures have usually excellent thermal properties, as they keep the structure cool in the summer and warm in the winter (ACI/TMS 122R-14, 2014). Although, masonry is generally a highly durable construction form, the materials used, the quality of the mortar, the workmanship and the pattern in which the units are arranged may substantially affect the performance of the overall masonry construction.

The design of new masonry structures according to the applicable code and their structural analysis through software programs available in the market require the value of the compressive strength f_{wc} of the masonry to be known. This value may be obtained by testing masonry prisms and wallettes or is estimated using semi-empirical formulas. In these formulas, data such as the compressive strength of the masonry units and the mortar that constitute the masonry are required. A dominant position among the first researchers involved in masonry structures is Engesser, who, in 1907, proposed in his work entitled Über weitgespannte Wölbbrücken, the first formulae for the estimation of masonry compressive strength considering the mortar and unit strengths. Thenceforth, a plethora of research work was carried out on compressive strength of masonry and numerous equations are available in the literature, as will be shown in the following sections. It is stressed that the objective is modern masonry, made with regular units and with an arrangement so that the masonry bond has limited influence on the compressive strength and complies with the code requirements (in most cases the usual staggered configuration given by running bond). Existing variations of masonry such as rubble masonry or dry-stacked masonry are out of the scope of the present paper.

Despite the plethora of research work in the last decades, the mechanics of masonry structures remains an open issue and, at the same time, a challenge for the practicing civil engineer. Furthermore, masonry strength as a function of the geometrical and mechanical characteristics of components is a subject not sufficiently explored, and more research is needed towards a robust and accurate prediction method. Considering the multiple geometrical and mechanical parameters of a masonry wall, which affect its compressive strength in a highly nonlinear manner, soft computing techniques emerge as the tool that can shed light on the prediction of masonry prism characteristics. This can assist in a better understanding of the material, as well as in design optimization processes in an integrated space, something that has not been possible until now.

Regarding the prediction of the compressive strength of masonry structures, an investigation based on a collection of 96 compressive tests on masonry was carried out by (Garzón-Roca et al. 2013). The authors used Artificial Neural Networks (ANNs) and Fuzzy Logic to forecast the compressive strength of masonry walls composed of clay masonry units and cement mortar. For their investigation they considered two parameters: the compressive strength of the unit and that of the mortar. In the same direction Zhou et al. (Zhou et al. 2016) used ANN and Adaptive Neuro-Fuzzy Inference System (ANFIS) models to forecast the compressive strength of hollow concrete block masonry and compared the predicted values to those obtained by experiments. Parameters such as height-to-thickness of the wall, the compressive strength of the masonry unit and the compressive strength of the mortar were used as input data, while the compressive strength of masonry was the output parameter. A major development with respect to modern masonry codes is that the material of the masonry unit is not being considered in the formulation, aiming at a novel and universal unified prediction.

More recently, Asteris et al. (Asteris et al. 2018) used back-propagation neural network models for the prediction of the compressive strength of masonry walls based on experimental data collected from the relevant literature (232 datasets). For this investigation, five parameters were used as input data, namely the volume fraction of masonry unit, the compressive strength of masonry unit and of the mortar, the height-to-thickness ratio of the masonry specimen and the volume ratio of bed joint mortar. According to the authors, the comparison of the derived results with the experimental findings demonstrates the ability of artificial neural networks to approximate the compressive strength of masonry walls in a reliable and robust manner. Finally, (Mishra et al. 2020, Mishra et al. 2021) used machine learning techniques as an alternative method for the prediction of compressive strength of masonry. The data used were obtained from experimental tests on masonry wallettes (direct

tests) and from non-destructive test (NDT) data (rebound hammer and ultrasonic pulse velocity tests), which were interpreted to determine the mechanical parameters of masonry. Three modelling approaches, namely fuzzy set, fuzzy logic, and neural network, were combined into the hybrid framework of a neuro-fuzzy modelling system and the predicted data were compared to those obtained by experiments.

In this context, in the work presented herein, the modelling of the compressive strength of single-leaf masonry walls has been investigated in-depth using soft-computing techniques. In particular, this study investigates both the application of Artificial Neural Networks (ANNs) and genetic programming (GP) models for the prediction of the compressive strength of masonry prisms. Specifically, for the development and the training of the computational models, a database consisting of 401 specimens taken from the literature was utilized. The masonry unit compressive strength f_{bc}, the mortar compressive strength f_{mc}, the masonry prism height-to-thickness ratio $\mathrm{h}_w/\mathrm{t}_w$ and the mortar thickness-to-masonry unit thickness ratio t_m/t_b were used as input parameters, while the value of the masonry prism compressive strength f_{wc} was used as output parameter. The optimum developed ANN model has proven to be successful, exhibiting very reliable predictions. Furthermore, compressive strength maps have been developed and are presented, revealing the nature of the compressive strength of masonry walls. These maps assist in the visualization of the effect of the different parameters on masonry compressive strength and can serve as a tool for educational purposes.

2. Literature review on masonry compressive strength

The enormous variety of masonry types can be characterized through parameters such as: (a) the type of the mortar (composition and quantity expressed through the joint thickness), (b) the nature of the material and form of the masonry units, (c) masonry construction procedure and

workmanship quality, and (d) the bonding properties between masonry units and mortar. It is well known that these parameters, together with the geometry of the tested specimen in compression, affect the mechanical properties of the material "masonry" (Hendry 1998). ,

In the following sections an attempt is made to highlight shortly the effect of the most representative parameters that affect single-leaf masonry's compressive strength, as well as to present the proposals developed by different researchers and adopted by International Codes that account the effect of these parameters on the compressive strength of masonry.

2.1 Relevant mechanical and geometrical parameters based on experimental works

With the purpose to assess the effect of selected parameters on masonry's compressive strength, previous research has included compression tests on prisms or wallettes (Figure 1). The possibility of testing two different types of specimens is also reflected in the standards that regulate the experimental determination of the compressive strength of masonry elements f_{wc}. In particular, the European standard EN 1052-1:1999 describes wallettes having specific geometry. The geometry of the specimen accounts for the effect of head joints. Additionally, the slenderness is such to avoid plate restraint effects on the measured strength. At least three identical specimens are constructed and tested in compression. Special care is taken after the construction of the specimens, in order to avoid drying of the specimen during the first days. For the estimation of the compressive strength of the wallette, the maximum load is divided by the gross cross-sectional area of the wallette. On the other hand, the American standard ASTM C1314 proposes a simpler configuration for testing masonry. In particular, stack bond prisms consisting of a sufficient number of stacked units are constructed and tested in compression. Prisms at least two masonry units' height are considered. A set of at least three prisms made of the same material are tested at the same age. It should be noted that in the case of ASTM C1314, the compressive strength of the prism is derived by dividing the

maximum load by the net cross-sectional area of that prism.

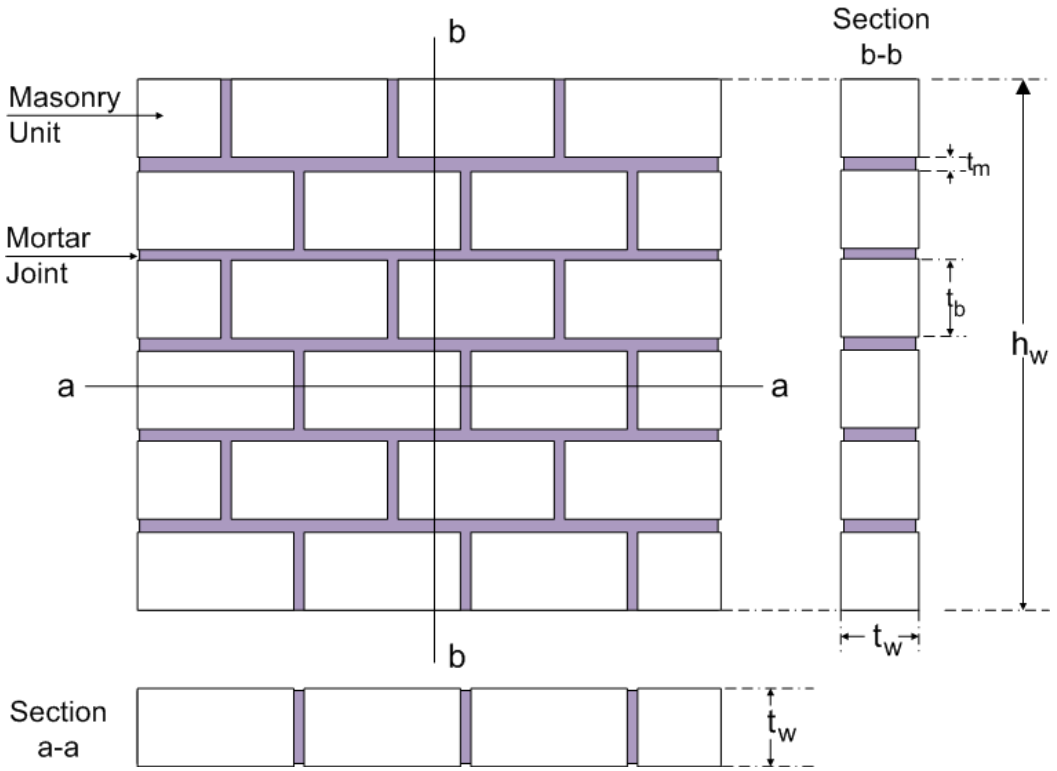

Figure 1. Geometry and notations of a masonry wall

The majority of the studies investigate the effect of the following parameters: (a) the compressive strength of masonry unit f_{bc}, (b) the compressive strength of the mortar f_{mc}, (c) the height-to-thickness ratio of the specimen and finally, (d) the ratio of masonry unit height to mortar bed joint thickness. Usually, the mortar is weaker than the masonry unit $(f_{mc}<f_{bc})$ and the behaviour of masonry in compression is governed either by the mortar confined compressive strength or by the strength of the unit under vertical compression and lateral tension. In such cases, f_{wc} values range between f_{mc} and f_{bc}, while an increase of the compressive strength of the constituent materials leads to an increase of the masonry strength (e.g. Kaushik et al. 2007, Lumantarna et al. 2014, Thamboo 2014, Zhou et al. 2016). For example, for the materials examined by (Kaushik et al. 2007), an increase of the order of 40% in f_{wc} is observed by increasing the value of f_{bc} by only 10%. However, an increase

of f_{bc} of the order of 30% leads to a disproportional increase of f_{wc} (of the order of 50%). Similarly, an increase of f_{mc} by 400% leads to an increase of f_{wc}, but only by 60-100% depending on the masonry unit. Finally, it is seen that the type of mortars determines the damage pattern observed in the masonry prisms as well as the post-peak behaviour. In particular, failure in masonry with a high-strength mortar is more brittle when compared to that with a low-strength mortar.

In case the compressive strength of units is smaller than the compressive strength of the mortar, the response of the masonry is controlled by the unit. In this case, compressive strength of masonry itself usually is lower than the compressive strength of both unit and mortar (e.g. Mohamad et al. 2007, Nagarajan et al. 2014, Balasubramanian et al. 2015, Ravula and Subramaniam 2017). The aforementioned effects of f_{bc} and f_{mc} on f_{wc} still apply (e.g. Thamboo 2014, Thaickavil and Thomas 2018).

Regarding the effect of the height-to-thickness ratio of the specimen on f_{wc}, it is found that the thinner mortar layers increase the bond strength between the mortar joint and the masonry unit, and thus, contribute to the increase in compression capacity of masonry. For the specific tested walls, this reduction is of the order of 30-40% (e.g. Thaickavil and Thomas 2018). Finally, an increase of the ratio of masonry unit height to mortar bed joint thickness on f_{wc} results in a decrease of the values of f_{wc}; e.g., for usual combinations of materials where $f_{bc}>f_{mc}$, a 50% decrease of the joint thickness can lead to a 10-20% reduction of f_{wc} (e.g. Reddy and Vyas 2008, Thamboo 2014).

2.2 Available proposals in the literature for strength prediction

2.2.1 Individual researchers

The prediction of the compressive strength of masonry walls f_{wc}, as well as its deformability characteristics (Young modulus of elasticity, Poisson ratio, σ-ε diagram, etc.),

have been the objective of several studies. Focusing on the compressive strength of modern masonry, analytical formulas have been developed by (Hilsdorf 1969), (Francis et al. 1970), (Tassios 1986) that consider the interaction between the masonry unit and mortar joint as a result of their different deformation characteristics. Two approaches have been adopted as the basis of failure theories: the first theory assumes plastic behaviour, whereas the second theory considers elastic behaviour, which in some cases is related to the behaviour of the unit and joint materials under the action of bi- or tri-axial stresses. These approaches simulate, in some cases, accurately the response of masonry under compression. However, the use of these formulas requires the deformability characteristics of the masonry unit and the mortar (such as Poisson ratio) to be known. These values are not usually available and, therefore, the use of these relationships is rather difficult.

Contrarily, most of the studies available in the literature propose empirical/mathematical models for the estimation of the compressive strength of masonry walls. These models are, in particular, based on the first formula proposed by (Engesser 1907), in which the compressive strength of masonry is related to the compressive strength of the masonry unit and of the mortar. The majority of studies propose linear or power expressions for the prediction of the compressive strength of masonry, such as:

$$f_{wc} = a f_{bc}^{m} + b f_{mc}^{n} \tag{1}$$

or

$$f_{wc} = c f_{bc}^{m} f_{mc}^{n} \tag{2}$$

where f_{bc}, f_{mc} are the compressive strength of masonry units and mortar, respectively and *a*, *b*, *c*, *m* and *n* are constants related to the specific materials and geometry under consideration.

In Table 1, the most representative equations from the literature are presented (namely, Equations 3 to 20), concerning the estimation of masonry prism or wallette compressive strength. It is noted that in these formulas, global effects, such as the slenderness of the wall, local-compression resistance, the thickness of mortar joint-to-height of the masonry unit ratio

(t_m/t_b ratio), or the effect of bi- or tri-axial stress on the constituent materials, are not considered.

Table 1. Empirical equations for the prediction of masonry compressive strength proposed by individual researchers

Nr	Formula	Equation	Reference	Method used
1	$f_{wc} = \frac{1}{3} f_{bc} + \frac{2}{3} f_{mc}$	(3)	(Engesser 1907)	RG
2	$f_{wc} = 0.68 f_{bc}^{1/2} f_{mc}^{1/3}$	(4)	(Bröcker 1963)	RG
3	$f_{wc} = 0.83 f_{bc}^{0.66} f_{mc}^{0.18}$	(5)	(Mann 1982)	RG
4	$f_{wc} = 0.317 f_{bc}^{0.531} f_{mc}^{0.208}$	(6)	(Hendry & Malek 1986)	RG
5	$f_{wc} = 0.275 f_{bc}^{0.5} f_{mc}^{0.5}$	(7)	(Dayaratnam 1987)	RG
6	$f_{wc} = 0.3 f_{bc}$	(8)	(Bennett et al. 1997)	RG
7	$f_{wc} = 0.3266 f_{bc} \times (1 - 0.0027 f_{bc} + 0.0147 f_{mc})$	(9)	(Dymiotis & Gutlederer 2002)	RG
8	$f_{wc} = 0.63 f_{bc}^{0.49} f_{mc}^{0.32}$	(10)	(Gumaste et al. 2007)	RG
9	$f_{wc} = 0.317 f_{bc}^{0.866} f_{mc}^{0.134}$	(11)	(Kaushik et al. 2007)	RG
10	$f_{wc} = 0.35 f_{bc}^{0.65} f_{mc}^{0.25}$	(12)	(Christy et al. 2013)	RG
11	$f_{wc} = 0.53 f_{bc} + 0.93 f_{mc} - 10.32$	(13)	(Garzón-Roca et al. 2013)	RG

12	$f_{wc} = \frac{84}{1 + e^{3.6 - 0.077 f_{mc} - 0.034 f_{bc}}} - 0.36$	(14)	(Garzón-Roca et al. 2013)	ANNs
13	$f_{wc} = 13.04 + 0.402 f_{bc}$	(15)	(Fortes et al. 2014)	RG
14	$f_{wc} = 0.75 f_{bc}^{0.75} f_{mc}^{0.31}$	(16)	(Lumantarna et al. 2014)	RG
15	$f_{wc} = 0.886 f_{bc}^{0.75} f_{mc}^{0.18}$	(17)	(Sarhat & Sherwood 2014)	RG
16	$f_{wc} = 1.34 f_{bc}^{0.1} f_{mc}^{0.33}$	(18)	(Basha and Kaushik 2015)	RG
17	$f_{wc} = 0.69 f_{bc}^{0.6} f_{mc}^{0.35}$	(19)	(Kumavat 2016)	RG
18	$f_{wc} = 0.25 f_{bc}^{1.09} f_{mc}^{0.12}$	(20)	(Thamboo and Dhanasekar 2019)	RG

f_{wc} is the masonry compressive strength; f_{bc} is the masonry unit compressive strength; f_{mc} is the mortar compressive strength.

Most proposals fail to consider the effect of the height-to-thickness ratio of the masonry prism, the volume fraction of mortar and of the brick, the effect of interfacial transition zone and bond strength, or the influence of the thickness of the joints on the compressive strength of masonry (Tassios & Chronopoulos 1986), (Tassios 1988), (Thaickavil & Thomas 2018). In particular, the semi-empirical formula proposed by (Tassios & Chronopoulos 1986) for the estimation of the compressive strength, f_{wc}, of one leaf stone or brick masonry, considers the effect of several parameters affecting the strength:

$$f_{wc} = \xi \cdot \left[(2/3\sqrt{f_{bc}} - a) + \beta \cdot f_{mc}\right] \tag{21}$$

where $\xi = 1/[1 + 3.5(k - k_o)]$ is a factor that takes into account the influence of the thickness of the joints and the volume fraction of the mortar, $k = V_m/V_{wall}$ is equal to the volume of mortar-to-volume of wall ratio, k_o is equal to 0.30, α is a factor that accounts the effect of the type and the shape of the masonry unit (α = 0.5 for brick units and stone blocks) and β is a factor that expresses the effect of the interfacial transition zone and bond strength between the masonry unit and the mortar (β = 0.5 for rough interfaces and β = 0.1 for very smooth-surface interfaces). According to the authors, this proposition should be applied for masonry with f_{mc} lower than 2.5MPa.

For well-built and regular masonry structures, (Tassios 1988) proposed the following expressions for the estimation of the compressive strength:

$$f_{wc} = \begin{cases} [f_{mc} + 0.4\,(f_{bc} - f_{mc})]\left(1 - 0.8\sqrt[3]{A}\right), & f_{bc} > f_{mc} \\ f_{bc}\left(1 - 0.8\sqrt[3]{A}\right), & f_{bc} < f_{mc} \end{cases} \tag{22}$$

where f_{bc}, f_{mc} are the compressive strength of masonry units and mortar, respectively, and $A = t_m/t_b$ is the ratio between the mean value of bed joint thickness t_m, and the mean value of the masonry unit height t_b.

The formula proposed by (Rozza 1995), presented in (Apolo & Martinez-Luengas 1995)

considers the effect of the compressive strength of the constituents' materials, as well as the relative fraction volume of the unit and of the mortar. In particular, f_{wc} is estimated by the equation:

$$f_{wc} = (v_u f_{bc} + 0.8 v_m f_{mc})/10 \quad (23)$$

where v_u is the relative volume of unit and v_m is the relative volume of mortar.

More recently, (Thaickavil & Thomas 2018) proposed a formula that considers the majority of the parameters that affect the masonry compressive strength. The authors carried out a regression analysis on a plethora of test data (232 datasets) within the following ranges: masonry unit strength from 3.1 to 127.0 MPa, mortar strength from 0.3 to 52.6 MPa and $□_w/t_w$ ratio from 1.15 to 5.75. Then, the following formula has been proposed:

$$f_{wc} = \frac{0.54 \times f_{bc}^{1.06} \times f_{mc}^{0.004}}{(□_w/t_w)^{0.28}} \quad (24)$$

where f_{bc}, f_{mc} are the compressive strength of masonry units and mortar, respectively, and $□_w/t_w$ is the height-to-thickness ratio.

2.2.2 International codes and standards

The form of the equations proposed by individual researchers have been adopted by international building codes and standards, usually not in terms of average values but adopting characteristic values (or the 5% quartile). This means that some care applied when comparing code and individual research expressions. Actually, the European Standard for the design of masonry structures (Eurocode 6, 2005 (EN 1996-1-1)) adopts a power model for the prediction of the compressive strength of masonry using the compressive strength of its components (see Equations 27 in Table 2). In these formulas, a *K* factor is introduced to consider the material and the voids of the masonry unit, as well as the type of the mortar. It should be

noted that the thickness of the mortar joint does not appear in the proposed formulas. The reason is that a predefined value for the thickness of joints is adopted (less than 15 mm for general purpose mortars and 1 to 3 mm for thin layer mortars). Thus, the influence of the thickness of the mortar joint has already been considered in the formulas and, therefore, is not taken as a parameter.

In the same line as above, in the MSJC (2013) standard, a linear model is adopted for the calculation of the compressive strength of masonry (Equation 26, Table 2), where f_{wc} is estimated only through the compressive strength of the masonry unit based on the gross cross-sectional area. On the contrary, the Australian code AS3700-2018 recognizes the significant effect of the height of unit-to-joint thickness ratio on the compressive strength of masonry. Therefore, it estimates the compressive strength of the masonry wall through a power model (Equation 25, Table 2) that accounts for the influence of the height of unit-to-joint thickness ratio through k_h factor and the type of unit, the mortar compressive strength and the bedding type (full or face shell) through k_m factor. Finally, in North American standards (TMS 402-11, CSA S304-14) tabulated values are provided for the calculation of the compressive strength of masonry based on the masonry unit strength and mortar type.

Table 2. Empirical equations for the prediction of masonry compressive strength adopted by International codes and standards.

Nr	Formula	Equation	Reference
1	$f_{wc} = k_h k_m {f_{bc}}^{0.5}$	(25)	AS 3700-2018
2	$f_{wc} = 2.758 + 0.2 f_{bc}$	(26)	ACI 530.1-02/ASCE 6-02/TMS 602-02 MSJC 2013
3	$f_{wc} = \begin{cases} K {f_{bc}}^{0.7} {f_{mc}}^{0.3}, & 3mm \le t_m \le 15mm \\ K {f_{bc}}^{0.85}, & t_m \le 3mm \end{cases}$	(27)	Eurocode 6, 2005 (EN 1996-1-1)

f_{wc} is the masonry compressive strength; f_{bc} is the masonry unit compressive strength; f_{mc} is the mortar compressive strength;

k_h is a factor in Australian code AS 3700-2018 that accounts for the ratio of unit height to mortar joint thickness, which should not exceed the value of 1.3; k_m is also a factor in Australian code AS 3700-2018 that accounts for the type of unit, the mortar compressive strength and the bedding type;

K is a constant in Eurocode 6, 2005 (EN 1996-1-1) formula, modified according to the National Annex for different countries. The value of this constant in the UK is 0.52 while in Greece *K* values range between 0.35 to 0.55 depending on the material and on the group of the masonry unit, the type of the mortar (e.g. general purpose mortar, thin layer mortar or mortar made with lightweight aggregates).

2.2.3 Research needs

In order to illustrate the broad range of f_{wc} values proposed by the studies available in the literature, the obtained curves were plotted in Figure 2. In particular, the f_{wc} values are depicted for mortar strength equal to 5 MPa. It is apparent from the figure that the range of f_{wc} values is too broad, especially for higher values of f_{bc} (in some formulas, limits apply). In fact, the lower bounds of the envelope are given by the propositions of (Hendry and Malek 1986; Dayaratnam 1987; Rozza 1995; Basha and Kaushik 2015), while the upper bound is given by that of (Engesser 1907; Fortes et al. 2014; Sarhat and Sherwood 2014; Lumantarna et al. 2014; Thaickavil and Thomas 2018; Thamboo and Dhanasekar 2019), while the propositions of the International Codes lie in-between (note that these are characteristic values and should be multiplied by 1.25 per (EN 1052-1 1998)). It is observed that the most conservative forecast among international codes is given by the Australian code. These findings further justify the need for additional research on the subject and for developing a more reliable and robust soft computing-based model for prediction of the compressive strength of masonry walls.

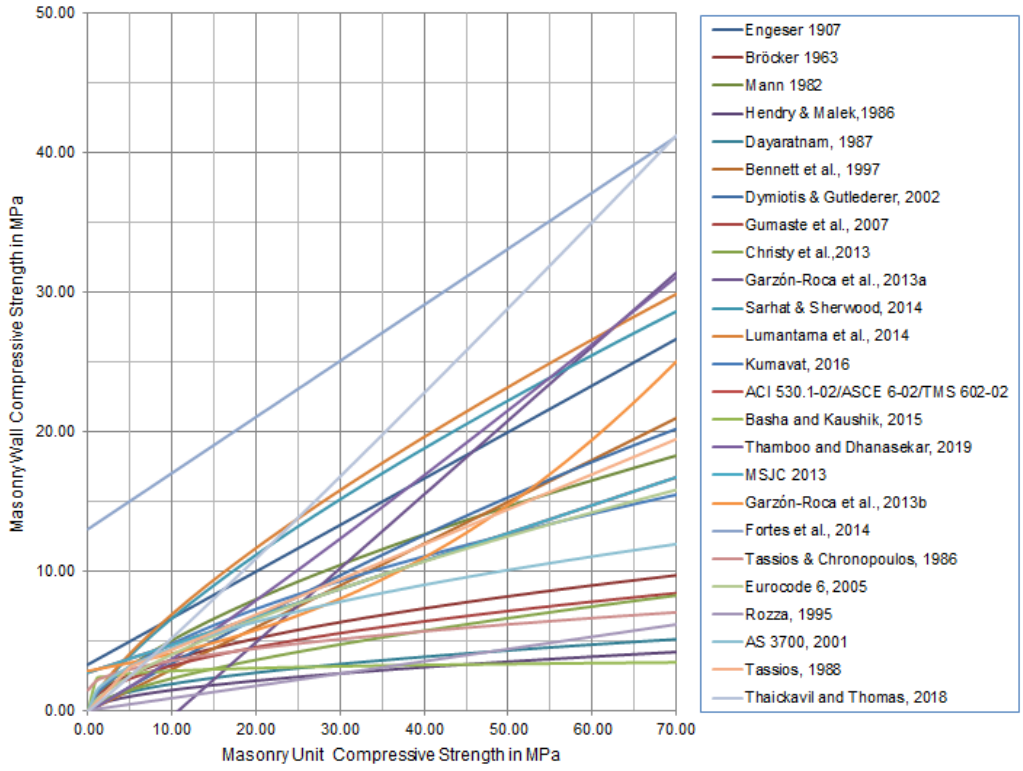

Figure 2. Masonry compressive strength based on different proposals with reference to a mortar compressive strength equal to 5 MPa.

3. Materials and Methods

3.1 Computational Predictive Models

This section presents the basic principles and constitutive models underpinning the computational predictive methods and techniques used in this research. Specifically, a brief review of the basic principles of Artificial Neural Networks (ANNs), with a specific focus on back-propagation neural networks (BPNNs), and Genetic Programming (GP) techniques will be presented.

3.1.1 Artificial Neural Networks

ANNs are advanced numerical models mimicking the structure and interaction of biological neural networks and were initially used for medicine research purposes to simulate strongly

nonlinear relationships between numerous input and ouput parameters (Wu et al. 1993, Anthimopoulos et al. 2016, Asteris et al. 2020, Rahimi et al. 2021, Gavriilaki et al. 2021). ANN models were subsequently introduced into the wider context of engineering disciplines (for example Gandomi and Alavi 2012, Le et al. 2021), which significantly enriched the mathematical backgound underpinning ANN.. At present, most neural network models presented in literature are structured on coarse elements of the biological neuron networks, and in this context it is expected that artificial neural network models will in the future be refined as the function underpinning biological neurons is advanced.

Artificial Neural Networks (ANNs) are information-processing models that are configured to learn and perform several tasks, such as classification, prediction, and decision-making. A trained ANN correlates a given input with a specific output, and it is therefore considered to be similar to a response surface method. The main advantage of a trained ANN over conventional numerical analysis procedures (such as regression analysis) is that the results are more reliable and require significant less computational effort (Samui 2008, Samui and Kothari 2011, Das et al. 2011, Hornik et al. 1989, Sadowski and Nikoo 2014, Asteris and Plevris 2013 and 2016, Cascardi et al. 2016, Cavaleri et al. 2017, Asteris et al. 2017 and 2019, Apostolopoulou et al. 2018, 2019 and 2020, Kechagias et al. 2018, Asteris and Mokos 2019, Armaghani et al. 2019, Cavaleri et al. 2019, Xu et al. 2019, Chen et al. 2019, Jiang et al. 2020).

In this research, a specific ANN type has been trained and developed, namely using back-propagation neural networks (BPNNs). A BPNN is a feed-forward, multilayer network (Hornik et al. 1989), in which information flows only from the input towards the output nodes with no feedback loops, and the neurons of the same layer are not connected to each other, but they are connected with all the neurons of the previous and subsequent layers. A BPNN has a standard structure that can be expressed as:

$$N - H_1 - H_2 - \cdots - H_{NHL} - M \tag{28}$$

where N is the number of input neurons (input parameters), H_i is the number of neurons in the i^{th} hidden layer for i = 1, …, NHL, where NHL is the number of hidden layers, and M is the number of output neurons (output parameters).

Despite the fact that the majority of researchers employing ANN techniques use multilayer NN models, ANN models comprising only one hidden layer can predict any forecast problem in a reliable and robust manner. A typical structure of a single node (with the corresponding R-element input vector) of a hidden layer is presented in Figure 3.

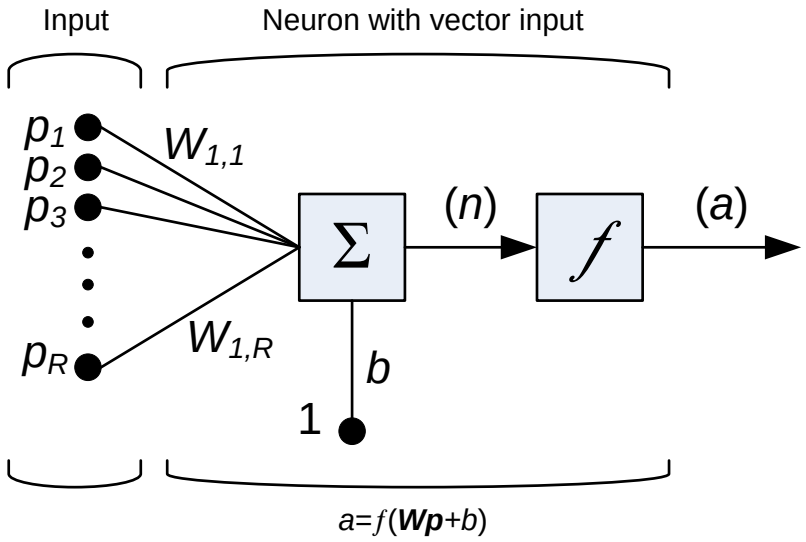

Figure 3. A neuron with a single R-element input vector

For each neuron i, the individual element inputs $p_1, \ldots, p_R$ are multiplied by the corresponding weights $w_{i,1}, \ldots, w_{i,R}$ and the weighted values are fed to the junction of the summation function, in which the dot product $(W \cdot p)$ of the weight vector $W = [w_{i,1}, \ldots, w_{i,R}]$ and the input vector $p = [p_1, \ldots, p_R]^T$ is generated. The threshold b (bias) is added to the dot-product forming the net input n, which is the argument of the transfer function f:

$$n = W \cdot p = w_{i,1}p_1 + w_{i,2}p_2 + \ \ldots + \ w_{i,R}p_R + b \tag{29}$$

The choice of the transfer (or activation) function f may significantly influence the complexity and performance of ANN. Although sigmoidal transfer functions are the most commonly used,

different types of functions are available. For example, Bartlett (1998) and Karlik and Olgac (2011) proposed a significant number of alternative transfer functions. In the present study, the Logistic Sigmoid and the Hyperbolic Tangent transfer functions were assumed to be more suitable for the specific research topic investigated. During the training phase, the training data are fed into the network which tries to create a mapping between the input and the output values. This mapping is achieved by adjusting the weights in order to minimize the following error function:

$$E = \sum (x_i - y_i)^2 \tag{30}$$

where x_i and y_i are the measured value and the prediction of the network, respectively, within an optimization framework.

In this research, an in-depth investigation was carried out based on (i) a plethora of different architectures and (ii) ten different activation functions which will be presented and discussed in depth in a next section. This resulted in 100 (10×10) different combinations being applied during the training and development process of the BPNNs.

3.1.2 Genetic Programming

The underlying principle of genetic programming (GP) techniques is associated with the natural selection and genetic recombination theory (Darwin 1859). In the context of soft computing techniques, the individuals in the population are assumed to be computer programs (Koza 1992). Genetic programming techniques operate by randomly generating a population of computer programs (Ramesh et al. 2020). Mutation, crossover, and reproduction take place during computation. Generation by GP iteratively transforms populations of programs into other populations of programs (Hajihassani et al. 2019).

In this soft computing technique, a random population of each individual (i.e. computer

programs) is generated to reach high multiplicity. A member is formed hierarchically by trial and error optimization of several functions. These functions are selected randomly by one or a set of functions such as for example Boolean logic functions (OR, NOT, AND, etc.), arithmetic operations (sum, divide, multiplication, substation, etc.) and trigonometric functions (sin, cos, tanh, etc.). All these functions operate on genetic concept such as reproduction, recombination (crossover) and mutation. Reproduction is carried out by copying an individual without affecting it. Recombination is carried out by changing genes between two individuals and mutation is carried out by exchanging part of randomly selected genes.

The terminating criteria used for genetic programming models are maximum population size, maximum number of generations, maximum tournament size, elite fraction, maximum number of genes, maximum tree depth and fitness value. Details of these criteria are discussed below in the results and discussion section. However, each criterion should be optimized carefully to deal with the local optima and global optima issues.

3.2 Gathering the Experimental Database

An adequate database should consist of reliable data, as well as of a sufficient quantity of data, covering the full range of parameter values, with regard to the parameters that influence the problem under investigation. According to Holický et al. (2016), a database is a compilation of various test sets, which should include all relevant parameter values, as well as all the information to allow assessing the quality and tolerances of the results. The following principles apply for establishing a test database, to define ranges of design parameters: (1) suitable identification of the measured strength, (2) correspondence between the test result and the failure mode as per the theoretical model, and (3) ability of the model to differentiate between various sub-divisions of a failure mode.

The demand for a reliable database is particularly crucial in databases compiled using

experimental results, in which high variations between experimental values are frequently observed, not only between experiments conducted by different scientists, but also between datasets derived from "identical" specimens, constructed by the same masons, cured under the same conditions and tested implementing the same standards and testing setup.

In light of the above, a large database has been composed within the present study. In particular, for the construction of the database used herein, 401 experimental datasets were employed from fifty-eight well known and reliable published experimental works, available in the literature (Table 3). All datasets used are based on specimens that have been prepared and tested in accordance with international standards. The parameters included in this database were: the mean value of the compressive strength of the masonry unit f_{bc} [in MPa], the mean value of the compressive strength of the mortar at the age of testing f_{mc} [in MPa], the slenderness of the masonry specimen expressed by the height-to-width of the specimen ratio, and the thickness of the mortar expressed by joint-to-height of the masonry unit ratio.

In the framework of the principles described above, for the preparation process of the database, masonry prisms and walls were considered. The specimens (each having from 2 up to 8 rows) were constructed by masonry units that were connected with thin or medium-thickness or thick joint mortar layer. The compositions of the mortars found in the literature were mainly cement based (with or without the addition of lime or soil). It was decided to include only experimental results related to specimens with mortar joints up to 20 mm. Several types of masonry units were found in the literature and the relevant test results were included in the database; namely, clay bricks, adobes, concrete blocks, compressed earth blocks, cement stabilized compressed earth blocks, calcium silicate bricks, several types of natural stones etc. The majority of the masonry units were either solid or units belonging to Group 1 (low volume of perforations) or 2 (moderate volume of perforations) according to Eurocode 6, 2005 (EN 1996-1-1).

It should be emphasized though that in case of hollow units filled with grout, only the results of grout having compressive strength similar with that of the units were included in the database. Furthermore, it is noted that the effect of the shape of the masonry unit used for the compression tests and, thus, the effect of the δ-factor (size effect) on the compressive strength of the unit, although included in the database, was not considered in the present investigation. For the maximum values of the compression strength of the masonry units and of the mortar, it was decided to adopt the limits from Eurocode 6, 2005 (EN 1996-1-1), namely f_{bc} and f_{mc} values up to 75 MPa and 20 MPa, respectively. Moreover, it was decided that the compressive strength of the masonry units, as well as the masonry prisms or wallettes in the database would be referred to the gross area of the specimens.

It should be stated that each dataset corresponds to a particular combination of different parameters. If several individual tests were performed for a given combination of parameters, then the database includes the mean values of the parameters and the mean value of the compressive strength of the masonry specimen. In this case, it is observed that the coefficient of variation (CoV) is in some cases up to 27%. Similar values of CoV were found for the compression test results of masonry prisms and wallettes having the same combination of parameters. It was decided to include the results of both specimens' configuration in the database, for completeness reasons as well as for further investigation. In general, despite their extensive exploitation in the present work, the measurements in the database can be further employed in other directions for future analysis.

Table 3. Data from experiments published in literature

Nr.	Reference	Number of Samples	Masonry Compressive Strength in MPa	Type of Unit
1	Thaickavil and Thomas 2018	48	0.73-2.80	CSEB, BCB
2	Ravula and Subramaniam 2017	1	5.80	SCWB
3	Singh and Munjal 2017	8	2.07-10.26	BCB, CoB
4	Zhou et al. 2016	12	5.48-14.60	HCB
5	Balasubramanian et al. 2015	1	2.82	B
6	Vindhyashree et al. 2015	1	4.42	SCoB
7	Lumantarna et al. 2014	12	6.19-30.79	VSCB
8	Nagarajan et al. 2014	3	1.92-2.43	BCB
9	Thamboo 2014	4	6.90-10.10	HCB
10	Vimala et al. 2014	12	0.65-3.20	SMB
11	Reddy and Vyas 2008	3	3.34-3.85	CEB
12	Kaushik et al. 2007	8	2.90-7.20	CoB
13	Gumaste et al. 2007	6	1.25-10.00	TMB
14	Mohamad et al. 2007	6	7.54-11.70	WC
15	Brencich and Gambarotta 2005	2	9.90-13.50	HCB
16	Bakhteri and Sambasivam 2003	4	10.89-16.89	SClB
17	Ip 1999	1	3.50	FS, B, OS
18	Hossain et al. 1997	1	18.20	BCB
19	Vermeltfoort 1994	29	3.90-26.90	WB, SMB, PMB, CSB
20	McNary and Abrams 1985	2	19.70-27.00	SMP, MCU
21	Francis et al. 1970	24	8.40-37.49	SB, EB
22	Gumaste et al. 2007	6	1.18-12.60	TMB, WB
23	N.C.M.A. 2012	26	6.98-16.46	HCB
24	Drougkas et al. 2016	6	9.05-13.80	SClB
25	Gayed et al. 2012	16	1.80-11.15	HCB
26	Vyas and Reddy 2010	3	5.01-6.32	CCB
27	Barbosa et al. 2010	3	10.00-12.00	HCB
28	Thamboo and Dhanasekar 2019	20	1.22-7.27	ClB, CEB

29	Mohebkhah 2007	1	7.66	SClB
30	Padalu et al. 2018	6	5.96-7.90	SClB
31	Muñoz et al.	1	9.84	SClB
32	Graus et al. 2019	1	22.90	GS
33	Zavalis et al. 2018	11	11.57-15.86	HCSB
34	Carvalho 2015	2	1.84-2.80	CEB
35	Oliveira 2014	4	2.62-4.05	CEB
36	Lourenço et al. 2013	1	5.37	PCoB
37	Medeiros et al. 2013	1	2.80	PCoB
38	Lourenço et al. 2010	1	5.26	PClB
39	Haach et al. 2010	2	5.44-5.95	PCoB
40	Vasconcelos and Lourenço 2009	1	37.00	GS
41	Mauro A. 2008	2	5.98-7.54	SClB
42	Mohamad 1998	8	7.54-11.70	HCB
43	Raposo et al. 2018	1	2.40	HCB
44	Cavaleri et al. 2012	3	7.42-9.05	HClB
45	Cavaleri and Di Trapani 2014	3	2.53-4.20	C
46	Cavaleri et al. 2014	1	1.74	HCL
47	Bosiljkov V. 2000	3	6.93-15.38	ClB
48	Gregoire 2007	4	1.57-11.03	CB, AC, AAC
49	Mishra et al. 2019	38	1.09-6.07	SClB
50	Furtado et al. 2016	7	0.45-0.97	HHClB
51	Furtado et al. 2020	9	0.54-1.28	HHClB
52	Shivaraj et al. 2014	1	4.21	HCoB
53	Sandeep et al. 2013	1	4.49	HCoB
54	Machado et al. 2019	9	4.35-12.04	CeU
55	Mohamad et al. 2011	4	5.25-9.27	CoB
56	Mohamad et al. 2007	1	8.24	CoB
57	Radovanović et al. 2015	4	2.16-3.10	ClB, CoB
58	Nwofor 2012	2	10.58-11.54	SBClB
	Total	**401**	**0.45-37.49**	

CSEB: cement stabilized earth block SClB: solid clay brick PClB: perforated clay block

BCB: burnt clay brick	FS: flagstone	C: calcarenite
SCWB: soft clay wire-cut brick	OS: Ohio stone	HLC: hollow lightweight concrete
CoB: concrete block	MB: adobe brick	ClB: clay brick
HCB: hollow concrete block	CSB: calcium silicate block	AC: dense aggregate concrete
B: brick	SMP: standard modular paver	ACC: autoclaved aerated concrete
SCoB: solid concrete block	MCU: modular cored unit	HHClB: horizontal hollow clay brick
VSCB: solid clay brick	CCB: compressed cement block	CeU: ceramic unit
SMB: stabilized adobe brick	ClB: clay brick	SBClB: solid burnt clay brick
CEB: compressed earth block	GS: granite stone	
TMB: table moulded brick	HCSB: hollow calcium silicate block	
WB: wire-cut brick	PCoB: perforated concrete block	

For the development of the soft computing model, input training vectors p (input parameters) with dimensions (1×6) are used consisting of: the value of the masonry unit compressive strength f_{bc}, the mortar compressive strength f_{mc}, the masonry specimen height-to-thickness ratio h_w/t_w, the mortar joint thickness t_m, the masonry unit height t_b and the mortar joint thickness to masonry unit thickness ratio t_m/t_b. The corresponding output training vector (output parameter) is of dimension (1 × 1) and consists of the value of the masonry compressive strength of walletes or prisms.

Table 4 presents the average, the minimum and the maximum values of the parameters included in the database, as well as the standard deviation (STD). It should be highlighted that some of the input variables may be dependent on each other.

Table 4 The input and output parameters used in the development of soft computing models

Nr.	Variable	Symbol	Unit	Category	Statistics			
					Min	Average	Max	STD
1	Masonry unit Compressive Strength	f_{bc}	MPa	Input	2.30	18.53	69.80	17.21
2	Mortar Compressive Strength	f_{mc}	MPa	Input	0.30	9.27	19.90	5.17
3	Masonry Prism height to thickness ratio	h_w/t_w	%	Input	1.15	3.47	8.60	1.21
4	Mortar thickness	t_m	mm	Input	0.51	11.24	20.00	3.02
5	Brick Thickness	t_b	mm	Input	36.00	115.02	250.00	59.41
6	Mortar thickness to masonry unit thickness ratio	t_m/t_b	%	Input	0.01	0.13	0.25	0.07
7	Masonry Compressive Strength	f_{wc}	MPa	Output	0.45	7.50	37.49	6.43

Consequently, as shown in Figure 4, the correlation coefficients between all possible variables were estimated. High correlation coefficient values (negative or positive) between

the input may lead to poor efficiency of the computational models and difficulty in interpreting the effects of the variables on the response. It is observed that besides t_m and (t_m/t_b) parameters, there is no significant correlation among the input parameters. On the contrary, the correlation coefficients between the input variables (parameters) and the output compressive strength parameter f_{wc}, must be strong in order to establish an accurate, robust and optimum ANN model. As shown in Figure 4, a very strong correlation between the masonry compressive strength f_{wc} and the masonry unit compressive strength f_{bc} exists: the correlation factor is of the order of 78%. The other correlation factors with the masonry compressive strength are relatively low.

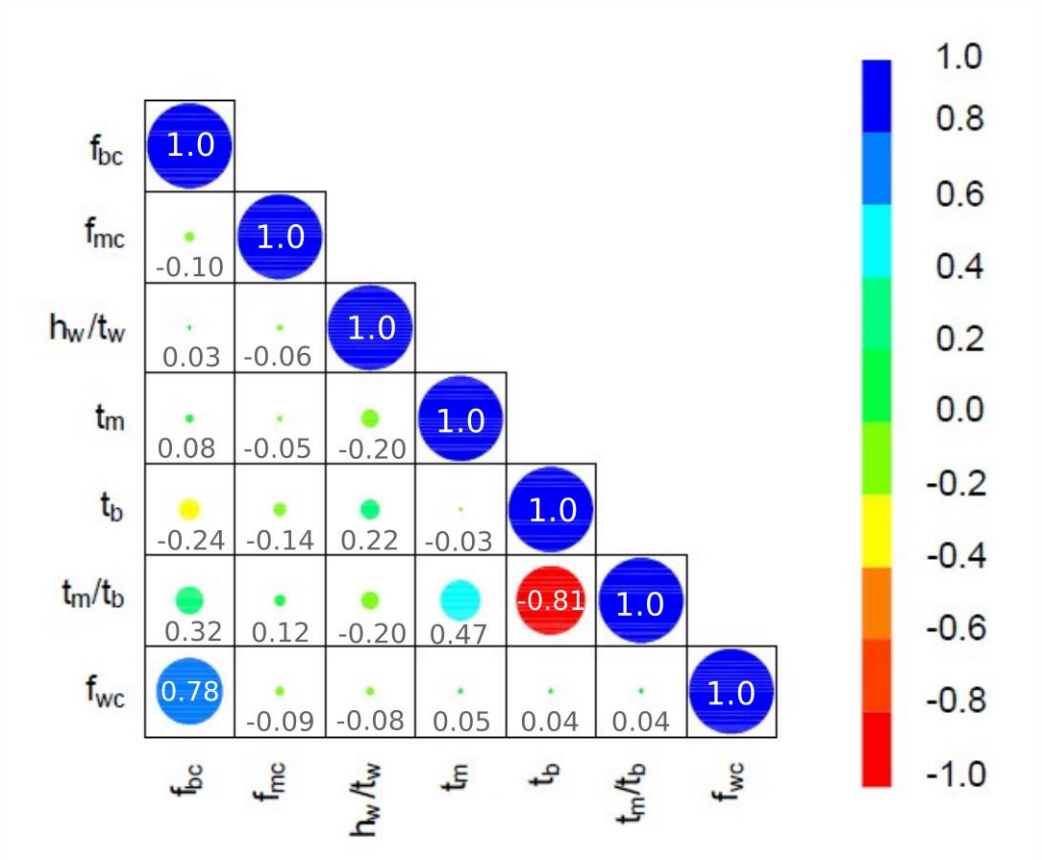

Figure 4. Correlogram of the variables (Input and Output parameters)

Furthermore, Figure 5 and Figure 6 depict the frequency histograms of the parameters

used for the modelling of masonry compressive strength. Significant insight can be gained from these figures, as potential ranges of the involved parameters, where the collected data are insufficient, become visually revealed. When sufficient data are available, covering a broad range of the parameter values, then the computational model can lead to a reliable prediction. On the contrary, when a certain range of an input parameter is not covered sufficiently or even lacks any data, the opposite usually occurs: the model does not have enough data to be trained successfully. In this context, the highlighted histogram areas where experimental data is lacking can provide the ground for future studies to investigate the aforementioned parameters, thus, not only leading to new experimental results, but also to enhancing the database.

As shown in Figure 5 and Figure 6, only 15% of all the datasets in the reviewed literature feature masonry units with f_{bc} values higher than 30 MPa. This can be attributed to the fact that medium and low strength masonry units are usually used for the construction of masonry buildings and thus, become more frequently a subject of investigation. Similarly, the vast majority (about 90%) of datasets represents specimens having h_w/t_w values between 2 and 6, as these values are dictated by the relevant testing standards for masonry walls. Likewise, a very high percentage (about 95%) of datasets refers to specimens with t_m values more than 8.0 mm (about 95%). These t_m values are usually used for the construction of loadbearing masonry. Overall, the database covers a wide range of input parameter values and is thus considered adequate for the development and training of the ANNs under investigation.

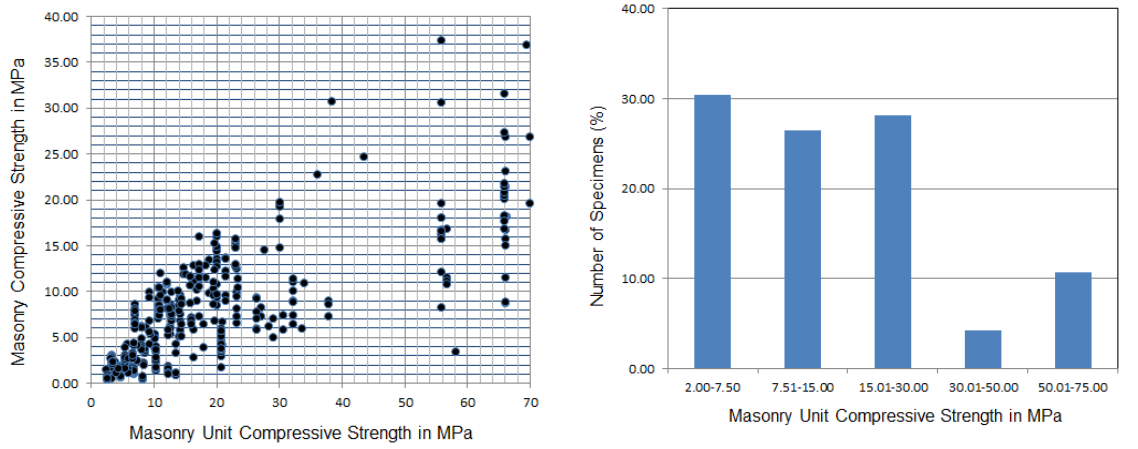

(a)

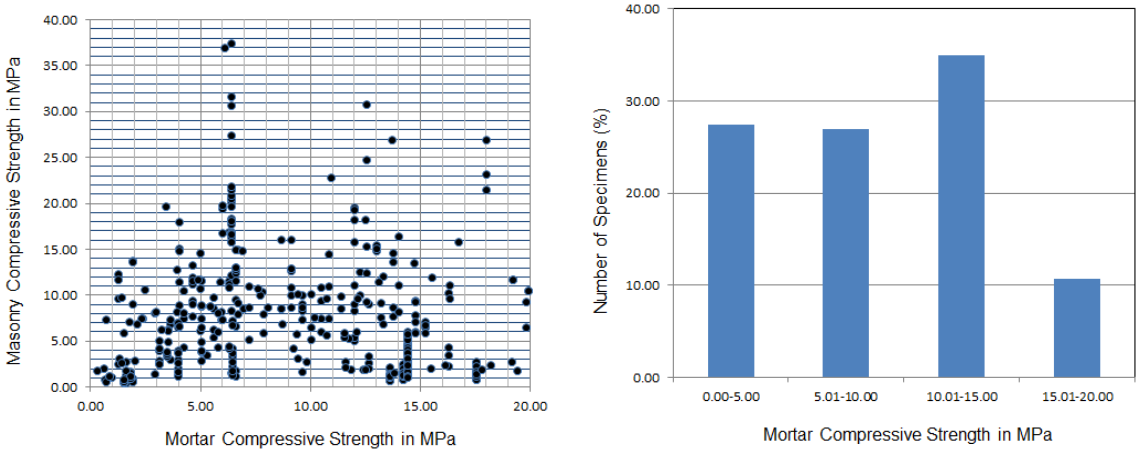

(b)

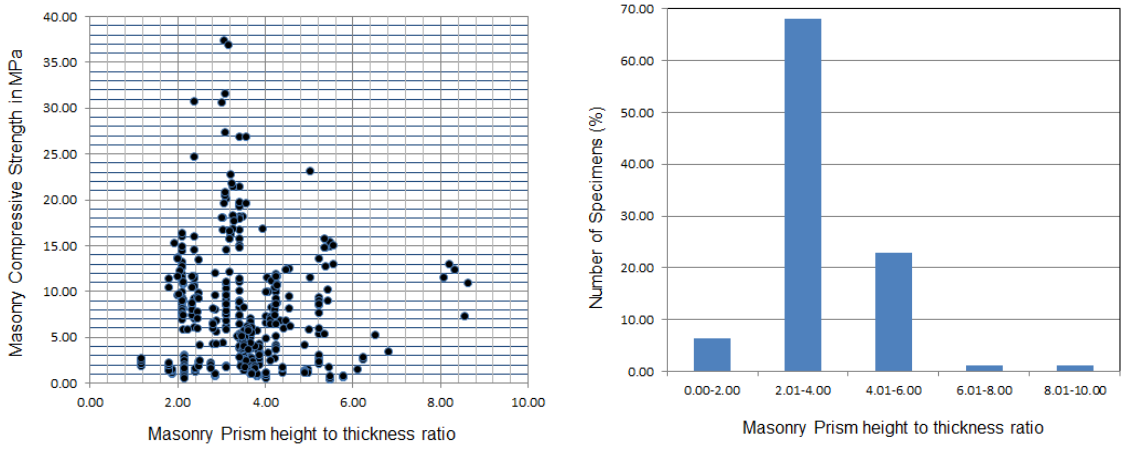

(c)

Figure 5. Histograms of parameters used for the prediction of masonry compressive strength for: (a) unit compressive strength, (b) mortar compressive strength, and (c) t_m/t_b ratio

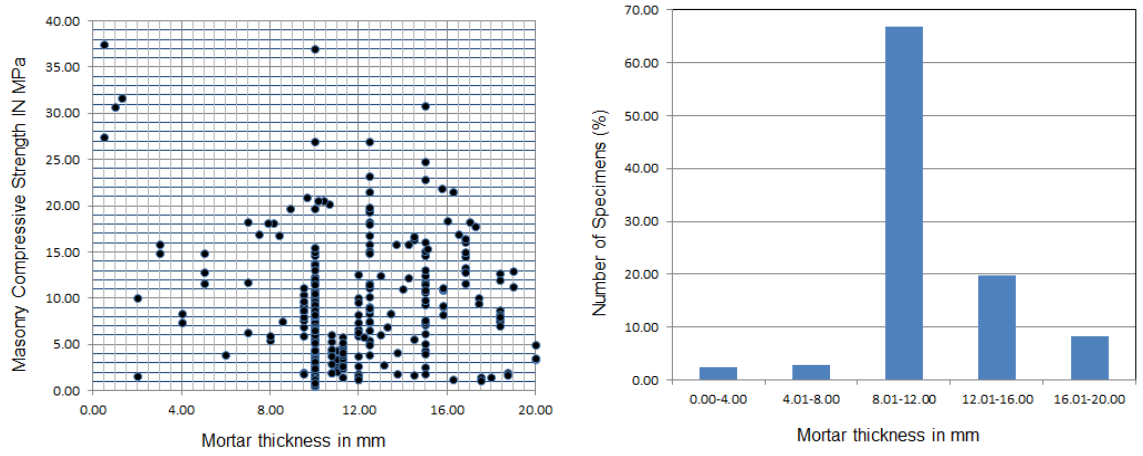

(a)

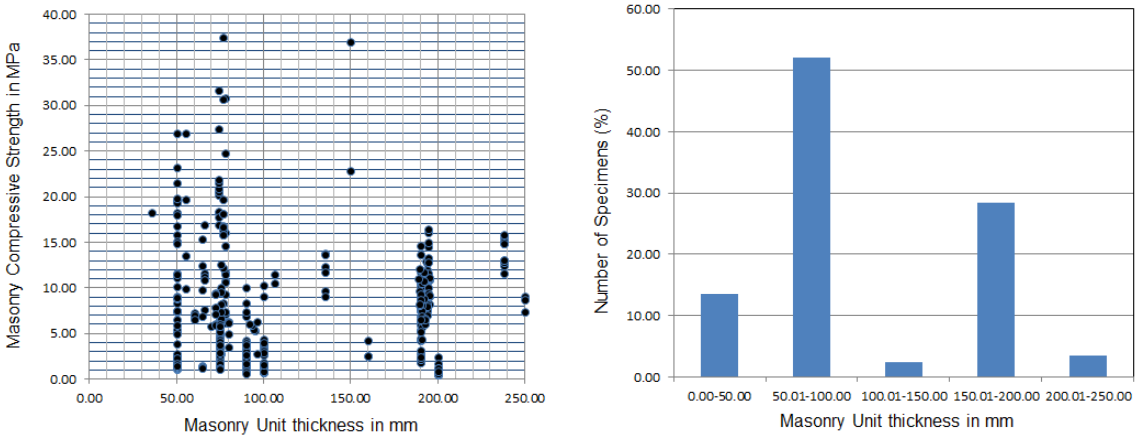

(b)

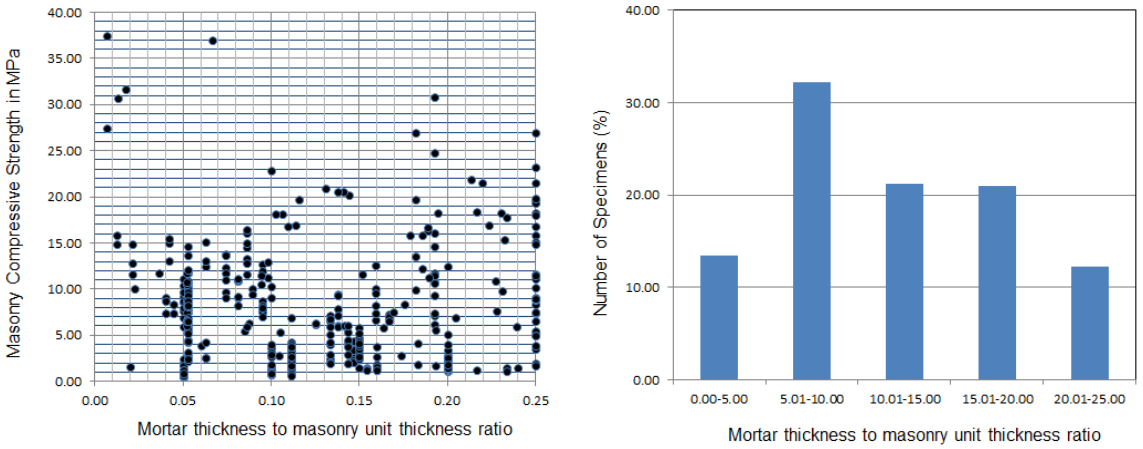

(c)

Figure 6. Histograms of parameters used for the prediction of masonry compressive strength for: (a) mortar thickness, (b) unit thickness, and (c) mortar to unit thickness ratio

3.3 Sensitivity analysis of the compressive strength based on experimental database

In general, sensitivity analysis of a numerical model is a technique used to determine if the output of the model is affected by changes in the input parameters. This will provide feedback as to which input parameters are the most significant, and thus, by removing the insignificant ones, the input space will be reduced and subsequently the complexity of the model as well as the training times required will be also reduced. In order to identify the effects of model inputs on the output, a sensitivity analysis (SA) can be conducted on the database. To perform the SA, the cosine amplitude method (CAM) which was used by many researchers (Khandelwal et al. 2016, Momeni et al. 2015 and Armaghani et al. 2015) was selected and implemented. In CAM, data pairs will be used to construct a data array, *X*, as follows:

$$X = \{x_1, x_2, x_3, \dots, x_i, \dots, x_n\} \tag{31}$$

Variable x_i in array, *X*, is a length vector of m as:

$$x_i = \{x_{i1}, x_{i2}, x_{i3}, \dots, x_{im}\} \tag{32}$$

The relationship between R_{ij} (strength of the relation) and datasets of x_i and x_j is presented by the following equation:

$$R_{ij} = \frac{\sum_{k=1}^{m} x_{ik} x_{jk}}{\sqrt{\sum_{k=1}^{m} x^2_{ik} \sum_{k=1}^{m} x^2_{ik}}} \tag{33}$$

The R_{ij} values between the compressive strength and the input parameters are shown in Figure 7. This analysis reveals that, among the parameters examined, the Unit compressive strength and the Mortar thickness have the greatest influence on compressive strength of

masonry walls, with strength values 0.90 and 0.74 respectively, followed by the Masonry prism height-to-thickness ratio, the Masonry unit thickness and the Mortar thickness-to-masonry unit thickness ratio. The Mortar compressive strength has the lowest impact on the compressive strength of masonry wall.

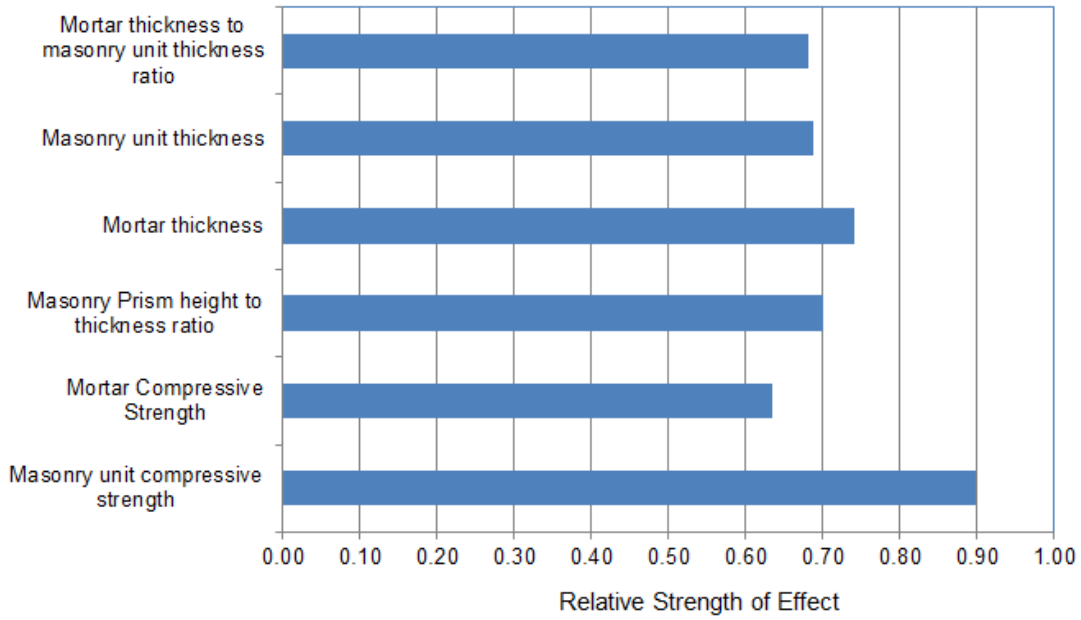

Figure 7. Sensitivity analysis of compressive strength on mechanical and geometrical mortar prism parameters based on experimental database

3.4 Performance Indices

Three different statistical parameters were employed to evaluate the performance of the derived model as well as first order linear equations available in the literature, including the root mean square error (*RMSE*), the mean absolute percentage error (MAPE), and the coefficient of determination (R^2). Lower *RMSE* and *MAPE* values represent more accurate prediction results (a null value indicates a perfect fit), while higher R^2 values represent a better fit between the analytical and predicted values (a zero indicates no fit and a unit value indicates a perfect fit). The aforementioned statistical parameters have been calculated using the following expressions (Alavi and Gandomi 2012):

$$RMSE = \sqrt{\frac{1}{n}\sum_{i=1}^{n}(x_i - y_i)^2} \tag{34}$$

$$MAPE = \frac{1}{n}\sum_{i=1}^{n}\left|\frac{x_i - y_i}{x_i}\right| \tag{35}$$

$$R^2 = 1 - \left(\frac{\sum_{i=1}^{n}(x_i - y_i)^2}{\sum_{i=1}^{n}(x_i - \bar{x})^2}\right) \tag{36}$$

where, n denotes the total number of datasets, and x_i and y_i represent the predicted and target values, respectively.

The reliability and accuracy of the developed neural networks were evaluated using R^2 and RMSE. RMSE presents information on the short-term efficiency which is a benchmark of the difference of predicated values in relation to the experimental values. The R^2 measures the variance that is interpreted by the model, which is the reduction of variance when using the model. It should be highlighted that, amongst the statistical indexes available, the majority of researchers use the R^2, in order to evaluate the effectiveness of the developed computation model. The R^2 is a measure of the linear correlation between two variables X and Y. For

forecasting models, such as AI models, X and Y represent the predicted and target values, respectively. According to the Cauchy–Schwarz inequality (Wu and Wu 2009), the coefficient R has a value between +1 and −1. The further away R is from zero, the stronger the linear relationship is between the two variables. The sign of R corresponds to the direction of the relationship. If R is positive, then as one variable increases, the other tends to also increase. If R is negative, then as one variable increases, the other tends to decrease. A perfect linear relationship (R = –1 or R =+1) means that one of the variables can be perfectly explained by a linear function of the other. As aforementioned, the reliability of a model's forecasting ability increases as the R^2 value approached the unit value.

When two forecasting models present different R values, as well as different slope values, comparison between the models is impossible. The same applies (even more so), when evaluating neural networks developed through different architectures. Therefore, the a20-index, has been recently proposed (Apostolopoulou et al. 2019, Asteris and Mokos 2019 and Armaghani and Asteris 2020) for the reliability assessment of the developed soft computing techniques:

$$\text{a20}-\text{index} = \frac{\text{m20}}{\text{M}} \tag{37}$$

where, M is the number of dataset sample and m20 is the number of samples with a value of (experimental value)/(predicted value) ratio, between 0.80 and 1.20. It should be stated that the adoption of the a20-index according to the range within ±20% is justified by the high values of the coefficient of variation observed in the results of compression tests of given masonry specimens. Note that for a perfect predictive model, the values of a20-index values are expected to be the unit value. The proposed a20-index has the advantage of a physical engineering meaning, as it declares the amount of the samples that satisfy the predicted values with a deviation of ±20%, compared to experimental values.

3.5 Methodology

In order to evaluate and find the optimal computational model for the prediction of the compressive masonry strength a number of individual steps were followed, as explained in detail hereafter:

Step 1. In the first step of the proposed methodology, a selection of the parameters that lead more successfully to the modelling of masonry compressive strength will be searched for. Specifically, a combination of the six input parameters (masonry unit compressive strength, mortar compressive strength, prism height to thickness ratio, mortar thickness, brick thickness, mortar to masonry unit thickness ratio) will be searched for, that leads to the more accurate estimation of the masonry compressive strength. For every possible combination of the six input parameters, a great number of ANNs will be created and trained, and the optimal will be selected as the one offering the best prediction.

Step 2. The selection of the optimal combination of parameters from the last step, determines the optimal ANN for the prediction of the masonry compressive strength. Based on its architecture and its final weight and bias values, an analytical expression can be formulated that describes the functionality of the ANN completely, and predicts the masonry compressive strength. The derivation of this analytical expression is particularly useful since it facilitates the implementation of the proposed model in software, without prior knowledge of the ANN technique.

Step 3. The parameters related with the selected optimal ANN, are also used as input parameters for the derivation of the optimal analytical expression, based on genetic programming, as described in a previous section.

Step 4. In this step, the optimal mathematical models are evaluated in terms of performance indices as well as regarding their numerical stability, particularly against overfitting. The best model is selected and semi-empirical expressions available in the literature, described previously, are also evaluated.

Step 5. In the last step, the proposed optimal model is employed for the prediction of the masonry compressive strength, parametrically investigating the influence of its relevant geometrical and mechanical properties and also producing relevant 2D and 3D maps/diagrams.

4. Results and Discussion

4.1 ANN models

4.1.1 Development and training

Different architecture ANNs were developed and trained, according to the following steps and parameters (summarized in Table 5):

- The 401 datasets comprising the database used for the training and development of the ANN models were divided into three separate sets. Specifically, 268 of 401 (66.8%) datasets were designated as Training datasets, 66 (16.5%) as Validation datasets, while 67 (16.7%) datasets were used as Testing datasets.
- During the training phase of the ANNs, the above datasets were used with and without normalization. In the case were normalization of the data was conducted, the minmax normalization technique in the range [0.10, 0.90] was implemented.
- The Levenberg–Marquardt algorithm (Lourakis 2005) was used for the training of the ANNs.
- 10 different initial values of weights and biases were applied for each architecture using the Matlab rand function.

- ANNs with only one hidden layer were developed and trained.
- The Number of Neurons per Hidden Layer ranged from 1 to 20, with an increment step of 1.
- Two functions, the Mean Square Error (MSE) and Sum Square Error (SSE) functions, were used as cost function, during the training and validation process.
- 10 functions, as presented in Table 5, were used as transfer or activation functions.

Model uncertainty may also influence the prediction of the structural resistance (e.g. Holický et al. 2016). Data-driven models are affected by epistemic and aleatoric uncertainties, the first ones due to limited data and knowledge on the modelled response, while the aleatoric uncertainties are related to a natural variability of the data concerning the input parameters. In this work, both types of uncertainties are implicitly considered in the processes for developing the proposed models while handling data, whereas a deeper study on this topic is beyond the scope of the present work.

In the present work, there is a series of datasets which was just used for testing the ANNs. These data could be used in some way to assess the model uncertainty. Note, however, that conventional approaches for uncertainty modelling, like Gaussian processes, are hardly scalable with larger data and lack the computational complexity of ANNs. A dropout approach would be possible, as it is applied at both training and test time. In this case, at test stage, the data is processed through the network several times, with different parameters being dropped at each run. Then, the outputs can be averaged over the several runs to output the probability, $P(Y|X)$, as well as the mean and CoV values of model uncertainty can be computed (e.g. Gal and Ghahramani 2016).

Table 5 Training parameters of ANN models

Parameter	Value	Matlab function
Training Algorithm	Levenberg-Marquardt Algorithm	trainlm
Normalization	Minmax in the range 0.10 – 0.90	mapminmax
Number of Hidden Layers	1	
Number of Neurons per Hidden Layer	1 to 20 by step 1	
Control random number generation	10 different random generation	rand(seed, generator), where generator range from 1 to 10 by step 1
Training Goal	0	
Epochs	250	
Cost Function	Mean Square Error (MSE) Sum Square Error (SSE)	mse sse
Transfer Functions	Hyperbolic Tangent Sigmoid transfer function (HTS) Log-sigmoid transfer function (LS) Linear transfer function (Li) Positive linear transfer function (PLi) Symmetric saturating linear transfer function (SSL) Soft max transfer function (SM) Competitive transfer function (Co) Triangular basis transfer function (TB) Radial basis transfer function (RB) Normalized radial basis transfer function (NRB)	tansig logsig purelin poslin satlins softmax compet tribas radbas radbasn

4.1.2 Optimum input parameters and model

In order to select the optimal combination of input parameters that results in a better prediction of the masonry compressive strength, according to the proposed methodology, four separate combinations of the geometrical and mechanical parameters, related to the prism, were examined, as shown in Table 6 The first combination (case I) takes into account only two input parameters, the masonry unit compressive strength f_{bc} and the mortar compressive strength f_{mc}. The second one (case II) considers three input parameters, the masonry unit compressive strength f_b, the mortar compressive strength f_{mc} and the masonry prism height-to-thickness ratio $\mathrm{h}_w/\mathrm{t}_w$. For the third combination (case III), also three input parameters are considered, the masonry unit compressive strength f_{bc}, the mortar compressive strength f_{mc} and the mortar thickness to masonry unit thickness ratio t_m/t_b, while the fourth combination (case IV) considers all four input parameters for the development and training of ANN models.

Table 6 Cases of ANN architectures based on the number of used input parameters

Case	Number of Input Parameters	Input Parameters			
		f_{bc}	f_{mc}	$\mathrm{h}_w/\mathrm{t}_w$	t_m/t_b
I	2	√	√		
II	3	√	√	√	
III	3	√	√		√
IV	4	√	√	√	√

For the presented parameters in Table 5 the development and training of 60.000 different architectures of ANN models was undertaken, for each one of the four different cases. It is worth to mention that the use of 10 different transfer functions alone, results in 100 different ANNs, for each architecture with the same number of neurons, as a result of the 100 (=10^2) different dual combinations of the 10 different transfer functions. The developed 60.000

ANNs for each one of the four cases were ranked based on the value of the RMSE performance index, for the Testing Datasets. The top 20 architectures are presented in Table A.1 to Table A.4 in Appendix A, while the optimum architecture of each one case is presented in Table 7. Among them, the optimum ANN model, based on the value of RMSE of Testing Datasets, is the BPNN 3-17-1 model that corresponds to the third case in Table 6, with three input parameters, the masonry unit compressive strength f_{bc}, the mortar compressive strength f_{mc} and the mortar thickness to masonry unit thickness ratio t_m/t_b. Specifically, the optimum BPNN 3-17-1 model (Figure 8) corresponds to a structure with three input parameters, 17 neurons and with use of normalization technique.

Based on the results presented in the Table 7, the following key findings are revealed, regarding the transfer functions of the hidden layer for all the optimum architectures. The most appropriate transfer functions for the hidden layer were the Normalized radial basis transfer function (NRB), the Radial basis transfer function (RB), the Triangular basis transfer function (TB) and the Symmetric saturating linear transfer function (SSL). All these transfer functions were rarely used by most of researchers for the development of ANN models. On the contrary, a common practice among the majority of researchers is to use the Hyperbolic Tangent Sigmoid transfer function (HTS) and the Log-sigmoid transfer function (LS).

Table 7 Best ANN architectures for each one case based on RMSE performance index for Testing Datasets

Case	Architecture	Normalization	Cost Function	Transfer Function		Random Number	Epochs	Performance Indices					
								Testing Datasets		Training Datasets		All Datasets	
				Hidden Layer	Output Layer			R	RMSE	R	RMSE	R	RMSE
I	2-28-1	yes	MSE	NRB	SSL	8	50	0.920	2.314	0.929	2.379	0.903	2.794
II	3-12-1	no	MSE	TB	SSL	7	27	0.937	1.960	0.883	3.043	0.891	2.931
1II	**3-17-1**	**yes**	**MSE**	**RB**	**HTS**	**4**	**49**	**0.951**	**1.757**	**0.970**	**1.561**	**0.948**	**2.052**
1V	4-24-1	no	MSE	SSL	HTS	2	12	0.949	1.818	0.950	2.019	0.946	2.091

HTS : Hyperbolic Tangent Sigmoid transfer function; SSL : Symmetric saturating linear transfer function; NRB : Normalized radial basis transfer function; RB: Radial basis transfer function ; TB: Triangular basis transfer function

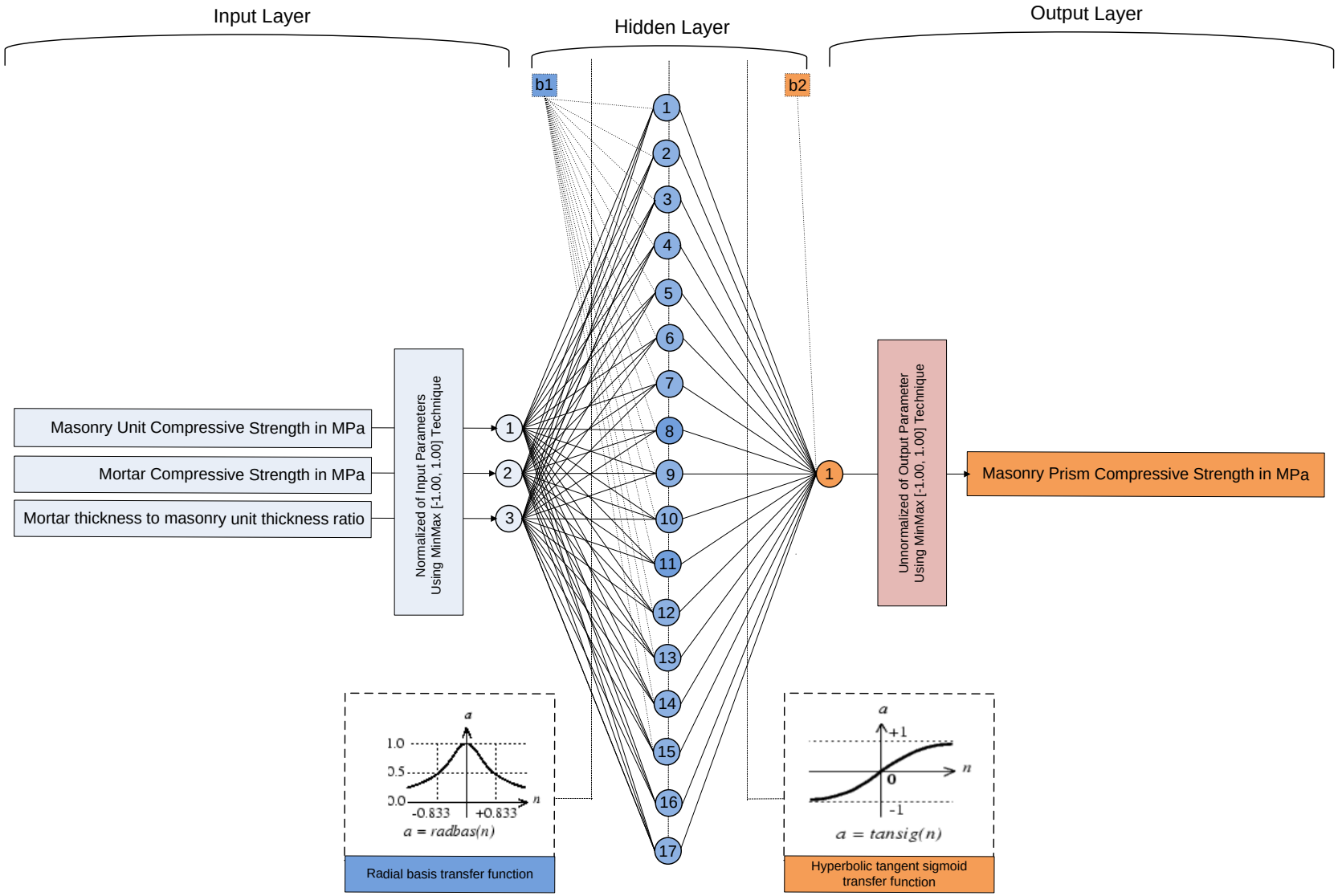

Figure 8. Architecture of the optimum BPNN 3-17-1 model

Furthermore, in Table 8 , Figure 9 and Figure 10, a detailed presentation of the performance of the optimum ANN model if given, that includes the a20-index. At this point, it should be stated that the most representative models are those more commonly adopted in several regions, particularly in design codes. The formulas proposed in this study are intended to be universal unified models, regardless of the masonry materials. The formulas can be applied to cases with values of parameters falling in the ranges considered in the database used to adjust the models.

Outliers are observed in Figure 9, which are in any case very limited. Outlying observations may be due either to the erraticism of the masonry materials or to the unconformity of experimental procedures. Different failure modes of similar specimens, for instance, due to defects in the masonry samples or to a nonconforming testing protocol, can lead to considerably different results, potentially resulting in outliers.

A potential outlier is scrutinized, when observing large deviation of an experimental result against the corresponding predictions (e.g., in Figure 9), by performing a deep analysis of the experimental response (damage trend and stress-strain evolution) amongst similar specimens in the considered dataset, to detect the cause of the deviation and decide if the experimental record should be considered an outlier.

The diagram in Figure 10 is aimed to assess (together with the performance indices) the reliability and the performance of the optimum BPNN model. It is verified that the developed optimum model is a reliable tool for the prediction of the masonry prism compressive strength, taking into consideration all 5 performance indices in Table 8.

Table 8 Summary of prediction capability of the optimum 3-17-1 BPNN

Model	Datasets	Performance Indices				
		a20-index	R	RMSE	MAPE	VAF
BPNN 3-17-1	Training	0.5709	0.9703	1.5609	0.2797	94.1382
	Testing	0.5373	0.9506	1.7572	0.3024	90.1892

	All	0.5362	0.9479	2.0521	0.3017	89.8133

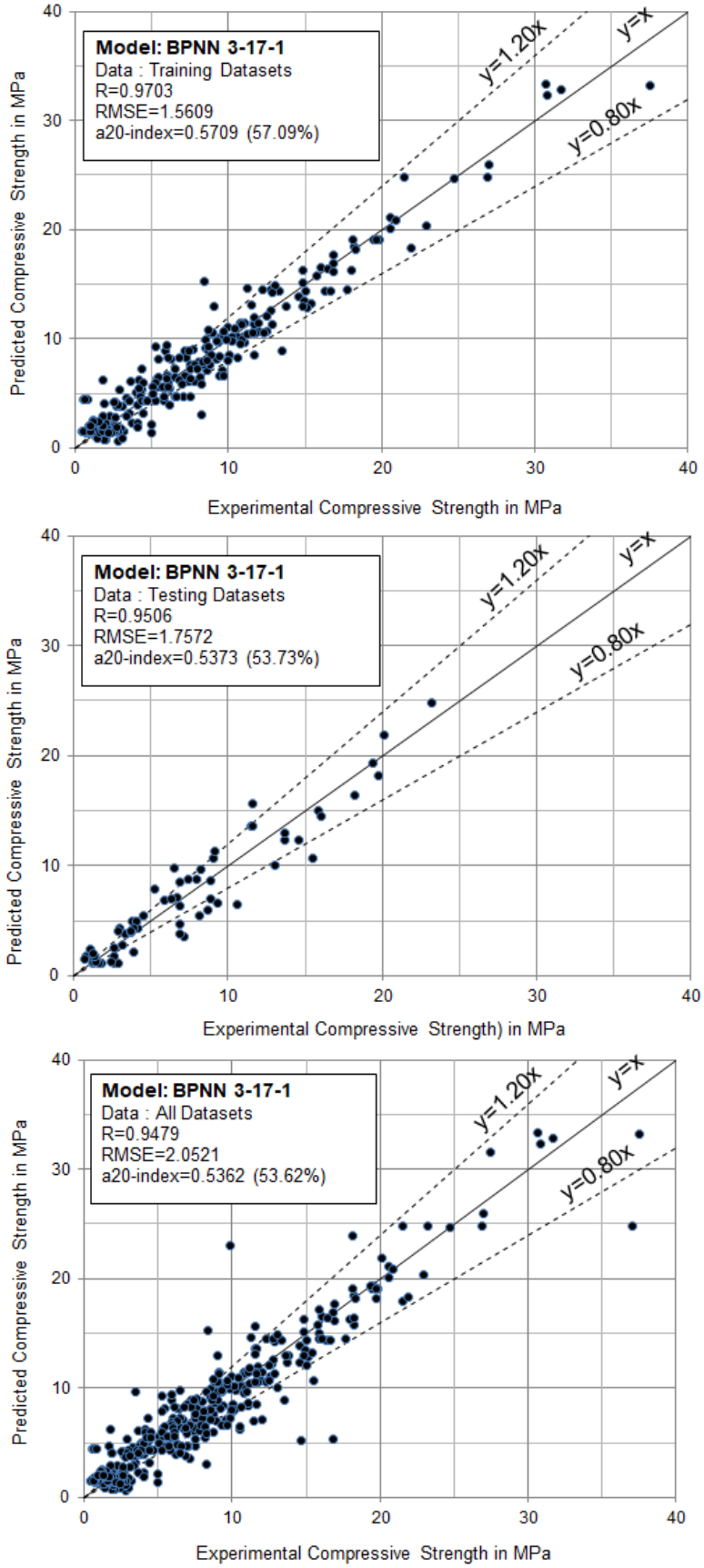

Figure 9. Experimental vs Predicted values of the masonry compressive strength for the optimum 3-17-1 BPNN model

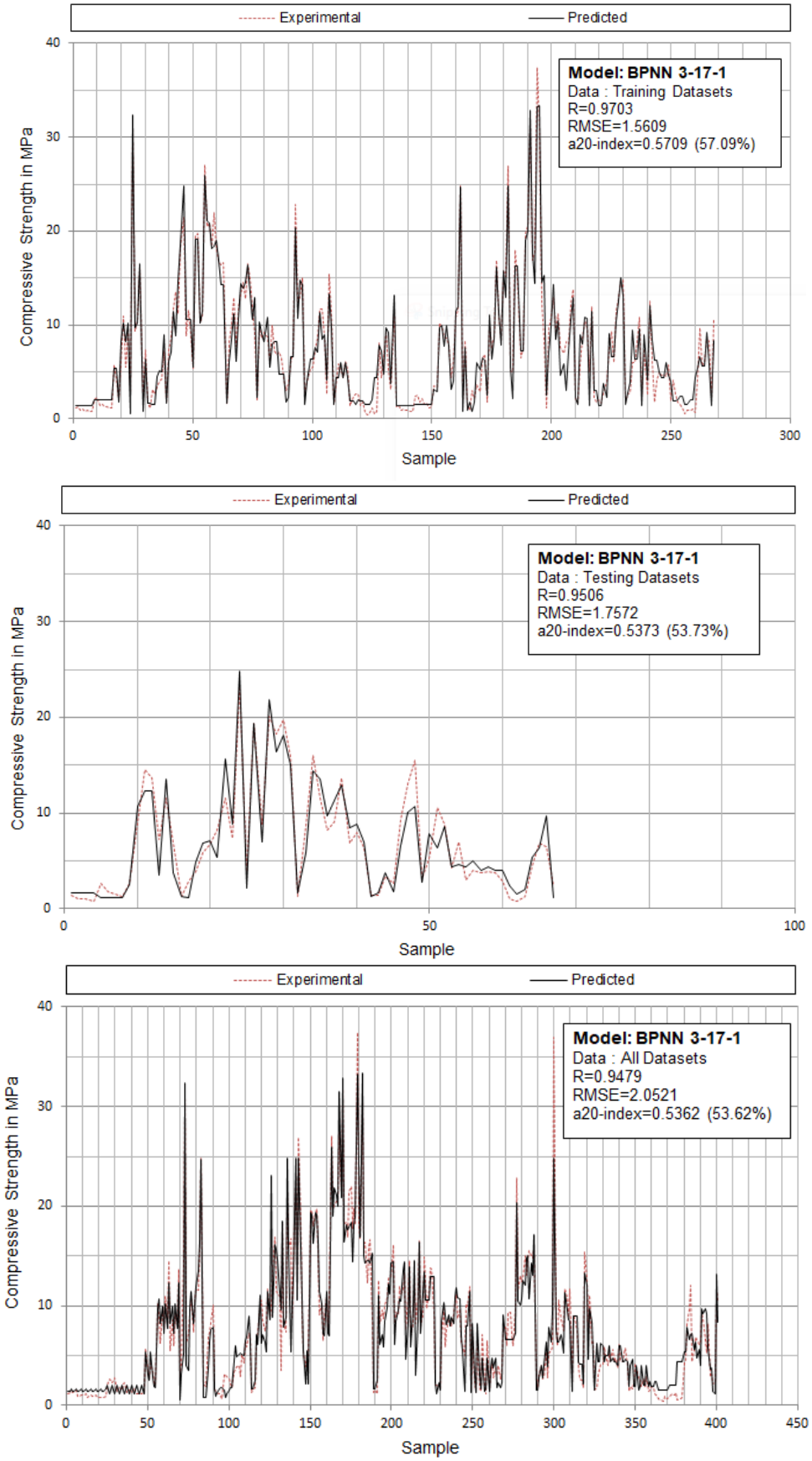

Figure 10. Experimental vs Predicted values of the masonry compressive strength for the optimum 3-17-1 BPNN model

4.1.3 Proposed explicit equation

In this section, a close form solution for the explicit equations to predict the masonry prism compressive strength is given, based on the optimal machine learning model presented. It is not convenient for engineers/researchers to use machine learning models in practice, because such a "black-box" model is composed of weights and bias, together with activation functions. Thus, explicit equations based on the developed machine learning model should be derived for a direct and efficient application. The proposed mathematic calculation for prediction of the masonry wall compressive strength f_{wc} in relation of the masonry unit compressive strength f_{bc}, the mortar compressive strength f_{mc} and the mortar thickness to masonry unit thickness ratio t_m/t_b is given in a matrix form by:

$$f_{wc} = \left(f_{wc}^{n} + 1\right)\left(\frac{max f_{wc} - min f_{wc}}{2}\right) + min f_{wc} \tag{38}$$

where f_{wc}^{n} is the normalized value of masonry compressive strength, defined by:

$$f_{wc}^{n} = tansig([L_W] \times [radbas([I_W] \times [IP] + [b_i])] + [b_0]) \tag{39}$$

where *tansig* is the Hyperbolic tangent sigmoid transfer function and *radbas* is the Radial basis transfer function, while $[I_W]$ is a 17×3 matrix containing weights of the hidden layer; $[L_W]$ is a 1×17 vector containing weights of the output layer; $[IP]$ is a 3×1 vector of the 3 Input Parameters, $[b_i]$ is a 17×1 vector containing the bias values of the hidden layer; and $[b_0]$ is a 1×1 vector containing the bias values of the output layer. All these matrices are given in Appendix B.

4.2 Genetic Programming based Expression

Based on the optimum combination of the parameters that mostly influence the value of the masonry prism compressive strength, an analytical closed form equation is investigated in this section. Specifically, using the Gene Expression Programming (GEP) method and the 401 experimental datasets, an equation was obtained for the prediction of the masonry prism compressive strength f_{wc} as a function of the masonry unit compressive strength f_{bc}, the mortar compressive strength f_{mc} and the mortar thickness to masonry unit thickness ratio t_m/t_b. To validate the modelling results, the available datasets were divided into two groups of training and validation/test datasets. Resulting from a trial and error method, two important features of the GEP configurations, namely the number of chromosomes and the number of genes were determined at 50 and 8, respectively. The relationships between the masonry compressive strength and the three input parameters, using GEP algorithm are implemented through MATLAB Code A**.1**, included in appendix.

The performance indexes of the proposed equation for the prediction of the masonry prism compressive strength f_{wc} as a function of the masonry unit compressive strength f_{bc}, the mortar compressive strength f_{mc} and the mortar thickness to masonry unit thickness ratio t_m/t_b, are shown in Table 9.

Table 9 Summary of prediction capability of the optimum GEP

Model	**Datasets**	**Performance Indices**				
		a20-index	**R**	**RMSE**	**MAPE**	**VAF**
GEP	Training	0.369	0.895	2.875	1.839	80.116
	Testing	0.313	0.896	2.491	0.556	79.854

	All	0.362	0.887	2.952	1.361	78.646

4.3 Comparison of the developed models and proposals in the literature

In Table 10, the statistical indices describing the performance of the two developed models and other proposals from the literature are reported. The models are sorted according to their a20-index. The proposed BPNN 6-7-1 model is ranked first among all models. Its performance is quite remarkable in terms of the a20-index, succeeding to predict the masonry compressive strength within a 20% margin of accuracy for a far greater number of specimens, compared to existing approaches. In fact, twice more specimens are well predicted by the BPNN 6-7-1 model, compared to the ACI 530.1-02/ASCE 6-02/TMS 602-02 and Eurocode 6, 2005 codes, and most of the other models. The proposed BPNN 6-7-1 model also performs better in terms of all other performance indices. For the RMSE index, the improvement is almost 40% compared to the best performing approach from the literature, which is proved the one by Mann (1982), in terms of RMSE. Similarly, the BPNN 6-7-1 model achieves a correlation coefficient R much closer to unity compared to any other model.

The alternative model developed in this paper, using the GEP apporach, is ranked second in terms of a20-index. Compared to Dymiotis & Gutlederer (2002) approach, which is the best performing model from the literature, in terms of a20-index, the GEP offers only a slight improvement. However, its performance is considerably better in terms of R coefficient and RMSE index, with a 30% reduction of RMSE compared to Dymiotis & Gutlederer (2002) and 25% from Mann (1982). Comparing the two developed models, the BPNN 6-7-1 and the GEP, the BPNN 6-7-1 scores a 71% increased a20-index and a 18% reduced RMSE compared to the GEP one.

A closer evaluation of the developed models has been undertaken, directly comparing their predictions with a key selection of experimental results from the database. The results are diagrammatically depicted in Figure 11 and Figure 12. Specifically, a set of specimens from

the same source (National Concrete Masonry Association, 2012), featuring varying unit compressive strength, has been selected for the evaluation of the developed BPNN 6-7-1 and GEP models, along with the best two performing models from the literature (Dymiotis & Gutlederer, 2002 and Tassios, 1988). The two diagrams differ in terms of mortar compressive strength (9.1MPa for the first and 4.6MPa for the second), while the mortar thickness to masonry unit thickness ratio remains constant. Such a reduction of the problem to a 2D space is valuable for the visualization of the fitting performance of the models and the uncovering of protentional numerical problems such as over-fitting, a deficiency that is not manifested through the statistical performance indices.

The general outlook from the two diagrams confirms that no overfitting occurs for either one of the two developed models, which present a smooth behaviour throughout the whole domain of the input values. The BPNN 6-7-1 model seems smoothly calibrated between the experimental values, while the GEP model seems to systematically underestimate the experimental value in the first diagram (i.e. for mortar compressive strength equal to 9.1MPa) and approximately averaging it in the second diagram (i.e. for mortar compressive strength equal to 4.6MPa). Both developed models present an improved overall fit to the experimental values, compared to the alternative models from the literature.

Table 10 Summary of prediction capability of the developed models against proposals in literature, based on a20-index and Testing Datasets

Datasets	Ranking	Model	Method	Performance Indices				
				a20-index	R	RMSE (MPa)	MAPE	VAF
All	1	BPNN 6-7-1	ANNs	0.536	0.948	2.052	0.302	89.813
	2	GEP	GP	0.313	0.896	2.491	0.556	79.854
	3	Dymiotis & Gutlederer, 2002	RG	0.299	0.806	3.560	0.572	64.590
	4	Tassios, 1988	RG	0.284	0.803	3.388	0.455	63.887
	5	ACI 530.1-02/ASCE 6-02/TMS 602-02	RG	0.269	0.797	3.748	0.505	57.644
	6	MSJC 2013	RG	0.269	0.797	3.758	0.508	57.644
	7	Mann 1982	RG	0.254	0.803	3.345	0.427	64.303
	8	Eurocode 6, 2005	RG	0.254	0.781	3.576	0.514	60.798
	9	Bennett et al., 1997	RG	0.239	0.797	3.931	0.717	63.390
	10	Garzón-Roca et al., 2013	ANN	0.239	0.631	5.433	0.556	13.317

RG: Regression Analysis

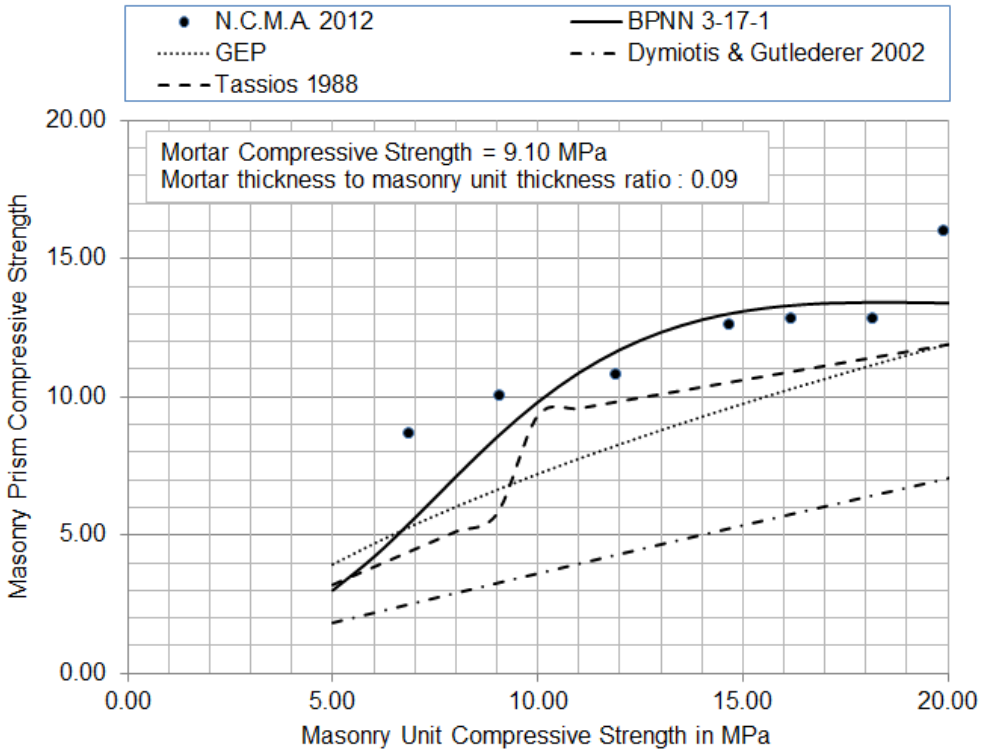

Figure 11. Comparison of developed models with experimental results and the three best proposals available in literature (mortar compressive strength equal to 9.1MPa)

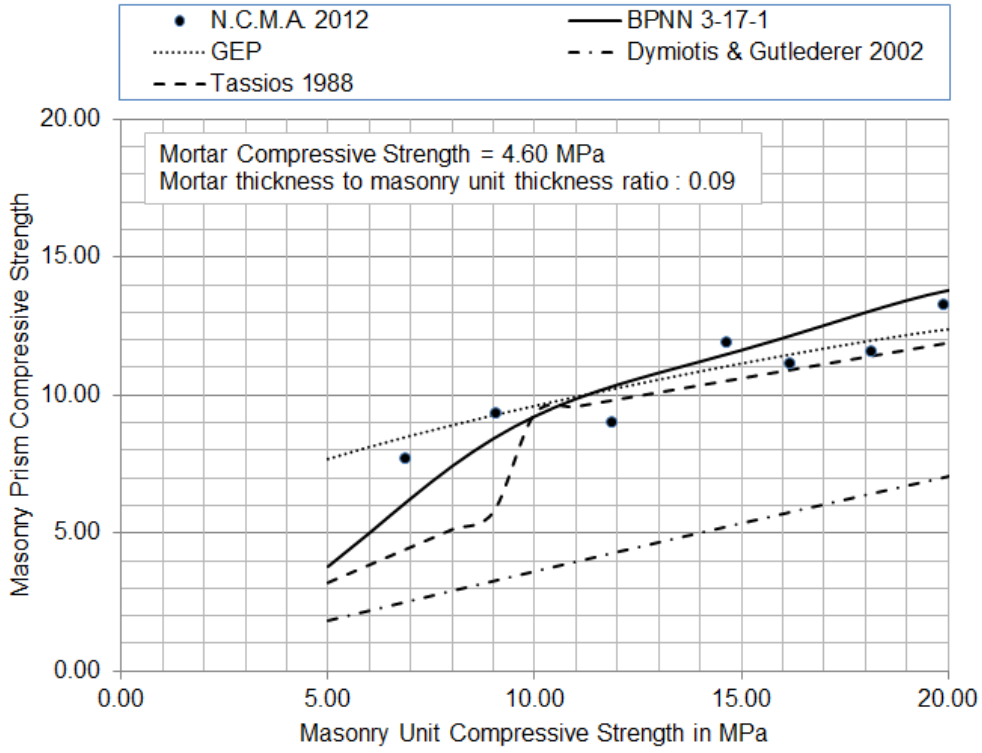

Figure 12. Comparison of developed models with experimental results and the three best proposals available in literature (mortar compressive strength equal to 4.6MPa)

4.4 Mapping of Masonry Compressive Strength

In this section, a mapping of the parameters that influence the masonry compressive strength is undertaken. Specifically, the maps in Figure 13 have been created using the optimal BPNN 3-17-1 model. The three maps depict the contours of the masonry compressive strength as a function of the unit compressive strength and the mortar compressive strength, under three distinctive and equally spaced values of the mortar thickness to unit thickness ratio (0.05, 0.10 and 0.15). Based on these maps, the following points can be made:

- The smoothness of the contours confirms that the proposed computational methodology does not suffer from overfitting, a commonly encountered problem during the development of ANN models. In case of overfitting, the model seems fitted quite close to the experimental data that are used for its training, however for slightly perturbated ranges of data the predictions become exceedingly worse,
- the highly nonlinear impact of the mortar compressive strength, for values of mortar compressive strength over 5 MPa, is indicated, as well as the nonlinear effect of the unit compressive strength for mortar strength values between 4.0 and 8.0 MPa,
- the mortar thickness to unit thickness ratio, whereas it is currently ignored in established approaches, it seems to significantly affect the masonry compressive strength,
- the proposed ANN is valuable not only for the reliable prediction of the masonry compressive strength, but also as a tool that demonstrates the way input parameters affect it. Thus, the proposed ANN can be a rather useful learning tool that reinforces the teaching of masonry mechanics.

However, a word of caution is needed regarding the applicability of ANN techniques. Before general conclusions can be made, a very broad experimental investigation is required in order to validate the ANN model predictions, particularly for these regions of the input parameters that lack a sufficient number of specimens. Such an investigation is indeed performed to the present work, yet for the range of parameters for which data is available.

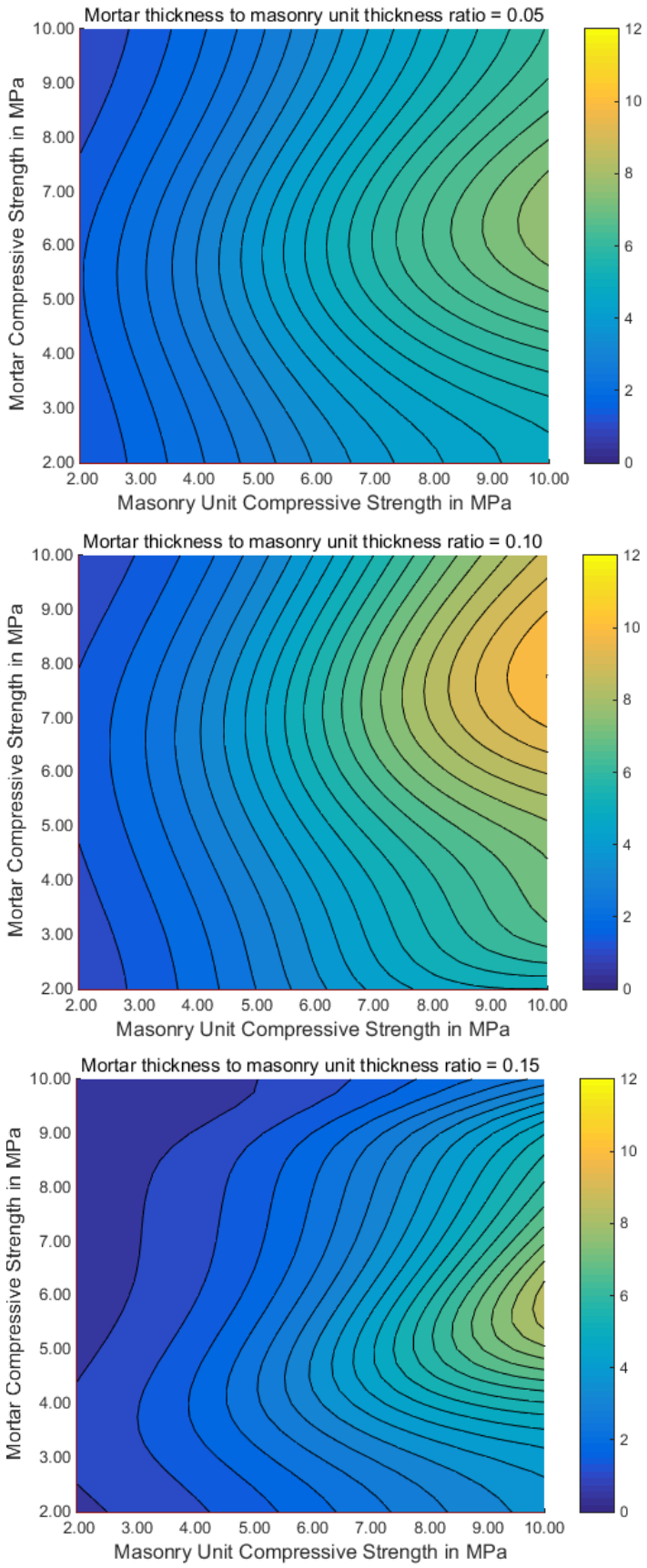

Figure 13. Mapping of the masonry compressive strength for the optimum 3-17-1 BPNN model

5. Conclusions

In the present paper, an artificial neural network was developed based on six parameters that influence the compressive strength of single-leaf masonry walls. A database of experimental specimens was compiled and used for the training and validation of the model.

From the results of sensitivity analysis, a very strong correlation is indicated between the masonry compressive strength and the masonry unit compressive strength, which is the most important influencing parameter. In addition to this parameter, the mortar thickness has the greatest influence on compressive strength of masonry walls, followed by the masonry prism height to mortar thickness ratio, the masonry unit height, and the mortar thickness to masonry unit height ratio. The mortar compressive strength has the lowest impact on the compressive strength of a masonry wall.

The obtained soft-computing models provide much better results than the expressions from literature. In particular, the ANN model provides a R for all dataset of 0.948, which compares to a best value of 0.806 for the literature expressions. Moreover, the proposed model predicts the masonry compressive strength within a 20% margin of accuracy, for more than half of the tests, which is almost twice the value from the literature expressions.

It should be stated that the proposed computational tool can become more accurate if more data are made available. Based on the data currently available, histograms have been obtained and revealed that the ANN model is more accurate for the whole range of mortar joint thickness to the masonry unit height ratio and for: (a) masonry units with compressive strength lower than 15 MPa, (b) mortars with compressive strength lower than 15 MPa, (c) masonry prism height-to-thickness ratio between 2 and 6, (d) mortar joint thickness between 8mm and 12mm and (e) masonry unit height between 50mm and 100mm, and 150mm and 200mm. It is therefore recommended that more data should be included in the database in

order to cover the full range of parameters considered in this investigation. Future systematic experimental studies should be carried out, particularly to cover the range of missing data, leading to new experimental results and the enhancement of the database. Such new results can be used to further train the ANN model, so that it is applicable to the entire range of parameters.

The approach here can also be applied to particular datasets with given ranges of material properties, through clustering or segmentation of the data (e.g., records with a f_{mc} significantly lower than the f_{bc} and/or with the highest t_m/t_b ratios, since in this case the mortar is the weakest and more significant portion of the masonry). The application, fine-tuning and evaluation of the approach in such cases is an interesting topic for future work. Likewise, the proposed approach can also be applied to the case of single leaf masonry walls in historical buildings, after making proper adjustments to fit the available experimental data and include the relevant input parameters.

Acknowledgements

The authors would like to express their sincere gratitude to Dr. Pere Roca, Professor at the Technical University of Catalonia, Dr. Vlatko Bosiljkov, Professor at the University of Ljubljana, Dr. Yogendra Singh, Professor at the Indian Institute of Technology Roorkee, Dr. Luca Pelà, Associate Professor at the Technical University of Catalonia, Dr. Liborio Cavaleri, Associate Professor at the University of Palermo, Dr. Amin Mohebkhah, Associate Professor at the Malayer University, and Dr. Dora Silveira, Postdoctoral researcher at the University of Porto, for providing experimental data related to masonry walls tested in compression.

Moreover, the authors would like to thank Dr. Gihad Mohamad, Professor at the Federal University of Santa Maria, Dr. André Lübeck, Adjunct Professor at the Federal University of Santa Maria, Dr. Còssima Cornadó, Postdoctoral researcher at the Technical University of Catalonia, and Dr. Anastasios Drougkas, Postdoctoral researcher at School of Civil Engineering, University of Leeds, for providing clarifications on their articles referenced in the present paper.

Appendix A

Table A.1. Top 20 best architectures for the Case I of input parameters for modelling the masonry compressive strength based on RMSE and Testing Datasets

Ranking	Architecture	Normalization	Cost Function	Transfer Function		Random Number	Epochs	Performance Indices					
								Testing Datasets		Training Datasets		All Datasets	
				Hidden Layer	Output Layer			R	RMSE	R	RMSE	R	RMSE
1	2-28-1	yes	MSE	radbasn	satlins	8	50	0.9197	2.3142	0.9294	2.3786	0.9025	2.7937
2	2-6-1	no	SSE	logsig	tansig	3	39	0.9089	2.3475	0.8542	3.3514	0.8561	3.3199
3	2-9-1	no	MSE	radbas	purelin	2	33	0.9110	2.3663	0.8907	2.9300	0.8968	2.8406
4	2-8-1	yes	SSE	radbas	tansig	1	49	0.9066	2.3674	0.8640	3.2471	0.8683	3.1852
5	2-4-1	no	MSE	logsig	tansig	2	50	0.9062	2.3743	0.8509	3.3864	0.8577	3.3035
6	2-16-1	no	MSE	radbas	tansig	3	39	0.9185	2.3758	0.9011	2.7973	0.9043	2.7420
7	2-4-1	yes	SSE	logsig	tansig	7	49	0.9050	2.3872	0.8484	3.4133	0.8559	3.3227
8	2-7-1	yes	MSE	logsig	satlins	3	49	0.9054	2.4032	0.8645	3.2423	0.8685	3.1823
9	2-4-1	no	MSE	logsig	tansig	7	39	0.9031	2.4091	0.8479	3.4177	0.8553	3.3286
10	2-26-1	yes	SSE	radbas	tansig	8	49	0.9218	2.4111	0.9362	2.2654	0.9135	2.6215
11	2-6-1	no	MSE	radbasn	purelin	4	39	0.9029	2.4150	0.8608	3.2815	0.8613	3.2626
12	2-5-1	yes	SSE	tribas	satlins	6	49	0.9031	2.4254	0.8500	3.3984	0.8502	3.3804
13	2-3-1	yes	SSE	radbasn	purelin	7	49	0.9008	2.4288	0.8419	3.4789	0.8447	3.4365
14	2-3-1	yes	MSE	radbasn	purelin	7	49	0.9007	2.4292	0.8419	3.4792	0.8447	3.4370
15	2-24-1	no	SSE	radbas	satlins	9	39	0.9052	2.4302	0.9161	2.5864	0.9129	2.6290
16	2-8-1	yes	MSE	softmax	tansig	4	49	0.9006	2.4337	0.8653	3.2314	0.8715	3.1493
17	2-4-1	yes	MSE	radbasn	satlins	5	49	0.9009	2.4372	0.8481	3.4162	0.8557	3.3232
18	2-23-1	yes	SSE	tansig	tansig	5	49	0.9054	2.4381	0.9250	2.4500	0.9186	2.5378
19	2-20-1	yes	SSE	softmax	tansig	2	49	0.9005	2.4396	0.8723	3.1519	0.8720	3.1426
20	2-3-1	no	SSE	radbasn	purelin	7	39	0.8997	2.4404	0.8420	3.4778	0.8446	3.4376

Table A 2. Top 20 best architectures for the Case II of input parameters for modelling the masonry compressive strength

Ranking	Architecture	Normalization	Cost Function	Transfer Function		Random Number	Epochs	Performance Indices					
								Testing Datasets		Training Datasets		All Datasets	
				Hidden Layer	Output Layer			R	RMSE	R	RMSE	R	RMSE
1	3-12-1	no	MSE	tribas	satlins	7	27	0.9367	1.9598	0.8831	3.0433	0.8906	2.9314
2	3-10-1	no	SSE	tribas	satlins	10	27	0.9383	1.9760	0.8829	3.0274	0.8807	3.0427
3	3-20-1	no	MSE	radbasn	tansig	6	47	0.9405	2.0451	0.9324	2.3359	0.9068	2.7356
4	3-19-1	no	MSE	tansig	purelin	8	27	0.9318	2.0454	0.9013	2.7924	0.8897	2.9314
5	3-11-1	no	MSE	tribas	tansig	1	39	0.9335	2.0546	0.9100	2.6730	0.9061	2.7183
6	3-9-1	no	SSE	poslin	purelin	7	47	0.9301	2.0566	0.8924	2.9092	0.8936	2.8827
7	3-12-1	no	MSE	satlins	satlins	1	13	0.9312	2.0579	0.9018	2.7881	0.8994	2.8156
8	3-27-1	yes	MSE	satlins	purelin	2	15	0.9304	2.0585	0.9035	2.7657	0.9036	2.7587
9	3-24-1	no	MSE	poslin	satlins	5	39	0.9307	2.0676	0.9198	2.5307	0.9170	2.5682
10	3-10-1	no	SSE	logsig	tansig	8	27	0.9298	2.0854	0.8936	2.8938	0.8942	2.8757
11	3-5-1	no	SSE	radbasn	satlins	7	27	0.9285	2.1036	0.8917	2.9183	0.8967	2.8509
12	3-18-1	no	MSE	poslin	purelin	2	39	0.9264	2.1127	0.8971	2.8486	0.8985	2.8195
13	3-8-1	yes	MSE	radbas	satlins	9	15	0.9291	2.1200	0.9003	2.8075	0.9029	2.7677
14	3-6-1	no	SSE	radbasn	satlins	6	47	0.9276	2.1233	0.8999	2.8114	0.8929	2.8928
15	3-17-1	yes	SSE	poslin	tansig	10	15	0.9251	2.1257	0.8985	2.8310	0.9018	2.7815
16	3-22-1	no	SSE	radbasn	tansig	2	39	0.9323	2.1288	0.9406	2.1887	0.9271	2.4106
17	3-29-1	no	MSE	tribas	tansig	1	39	0.9289	2.1365	0.9074	2.7156	0.9024	2.7771
18	3-14-1	yes	SSE	radbasn	purelin	3	15	0.9270	2.1415	0.9371	2.2510	0.9328	2.3168
19	3-10-1	yes	SSE	satlins	satlins	9	15	0.9237	2.1428	0.8853	2.9984	0.8858	2.9809
20	3-14-1	no	MSE	radbas	tansig	1	39	0.9248	2.1483	0.9123	2.6426	0.9002	2.7972

Table A.3. Top 20 best architectures for the Case III of input parameters for modelling the masonry compressive strength

Ranking	Architecture	Normalization	Cost Function	Transfer Function		Random Number	Epochs	Performance Indices					
								Testing Datasets		Training Datasets		All Datasets	
				Hidden Layer	Output Layer			R	RMSE	R	RMSE	R	RMSE
1	3-17-1	yes	MSE	radbas	tansig	4	49	0.9506	1.7572	0.9703	1.5609	0.9479	2.0521
2	3-28-1	yes	SSE	tribas	satlins	8	12	0.9394	1.9953	0.9615	1.7856	0.9354	2.3081
3	3-18-1	yes	SSE	tribas	satlins	10	12	0.9335	2.0207	0.9498	2.0162	0.9394	2.2049
4	3-27-1	no	MSE	softmax	satlins	7	49	0.9325	2.0216	0.9164	2.5825	0.9170	2.5682
5	3-26-1	yes	SSE	tribas	purelin	2	6	0.9299	2.0577	0.9500	2.0144	0.9392	2.2043
6	3-9-1	yes	MSE	satlins	satlins	1	29	0.9306	2.0602	0.9100	2.6735	0.9082	2.6894
7	3-24-1	no	SSE	poslin	purelin	10	49	0.9297	2.0651	0.9119	2.6524	0.9149	2.5955
8	3-28-1	yes	SSE	softmax	purelin	3	6	0.9323	2.0715	0.9342	2.3002	0.9325	2.3189
9	3-14-1	yes	SSE	poslin	purelin	10	12	0.9291	2.0748	0.9055	2.7371	0.9074	2.6986
10	3-13-1	yes	SSE	poslin	tansig	9	12	0.9298	2.0759	0.8993	2.8204	0.9018	2.7808
11	3-18-1	yes	MSE	softmax	purelin	2	29	0.9341	2.0793	0.9317	2.3496	0.9315	2.3447
12	3-13-1	no	MSE	tansig	purelin	9	49	0.9284	2.0795	0.9245	2.4582	0.9225	2.4779
13	3-13-1	yes	SSE	tribas	purelin	5	6	0.9283	2.0858	0.9341	2.3012	0.9306	2.3550
14	3-9-1	yes	SSE	radbasn	satlins	5	6	0.9314	2.0884	0.9325	2.3283	0.9143	2.6085
15	3-24-1	yes	MSE	tribas	tansig	2	29	0.9319	2.0916	0.9425	2.2002	0.9210	2.5548
16	3-16-1	no	SSE	satlins	tansig	4	10	0.9281	2.0929	0.9269	2.4215	0.9250	2.4461
17	3-30-1	no	SSE	satlins	tansig	6	49	0.9273	2.0934	0.9437	2.1359	0.9392	2.2055
18	3-18-1	no	MSE	poslin	satlins	3	20	0.9275	2.0974	0.9425	2.1544	0.9368	2.2493
19	3-9-1	yes	SSE	tribas	satlins	7	6	0.9273	2.0979	0.8920	2.9330	0.8965	2.8607
20	3-9-1	no	MSE	softmax	purelin	8	49	0.9265	2.1121	0.9146	2.6114	0.9180	2.5506

Table A.4. Top 20 best architectures for the Case IV of input parameters for modelling the masonry compressive strength

Ranking	Architecture	Normalization	Cost Function	Transfer Function		Random Number	Epochs	Performance Indices					
								Testing Datasets		Training Datasets		All Datasets	
				Hidden Layer	Output Layer			R	RMSE	R	RMSE	R	RMSE
1	4-24-1	no	MSE	satlins	tansig	2	12	0.9485	1.8183	0.9500	2.0193	0.9464	2.0910
2	4-6-1	yes	MSE	satlins	satlins	9	15	0.9457	1.8277	0.9287	2.3912	0.9313	2.3407
3	4-8-1	no	SSE	tansig	purelin	7	12	0.9441	1.8553	0.9385	2.2286	0.9341	2.2935
4	4-9-1	yes	SSE	tribas	purelin	2	10	0.9434	1.8625	0.9296	2.3794	0.9239	2.4591
5	4-10-1	yes	SSE	logsig	tansig	9	10	0.9464	1.8637	0.9261	2.4380	0.9269	2.4184
6	4-21-1	yes	SSE	poslin	satlins	7	10	0.9437	1.8665	0.9432	2.1491	0.9385	2.2301
7	4-17-1	no	MSE	poslin	tansig	3	12	0.9448	1.8711	0.9243	2.4833	0.9212	2.5190
8	4-9-1	no	SSE	satlins	tansig	2	12	0.9423	1.8806	0.9356	2.2784	0.9340	2.2948
9	4-23-1	no	MSE	softmax	tansig	5	12	0.9422	1.8864	0.9307	2.3656	0.9290	2.3818
10	4-20-1	yes	MSE	satlins	satlins	6	10	0.9417	1.8964	0.9560	1.8907	0.9466	2.0733
11	4-7-1	yes	MSE	tribas	tansig	10	15	0.9422	1.9007	0.9283	2.4020	0.9299	2.3726
12	4-10-1	no	MSE	tansig	tansig	9	12	0.9407	1.9019	0.9465	2.0798	0.9396	2.2007
13	4-7-1	yes	MSE	poslin	satlins	7	10	0.9413	1.9121	0.9158	2.5887	0.9187	2.5353
14	4-4-1	no	SSE	radbas	tansig	8	12	0.9415	1.9149	0.9133	2.6271	0.9164	2.5725
15	4-16-1	no	SSE	satlins	satlins	8	12	0.9419	1.9151	0.9313	2.3508	0.9338	2.3062
16	4-17-1	no	MSE	tansig	tansig	8	12	0.9397	1.9238	0.9293	2.3882	0.9305	2.3551
17	4-18-1	yes	SSE	poslin	satlins	4	10	0.9390	1.9259	0.9378	2.2388	0.9357	2.2697
18	4-5-1	yes	MSE	radbas	satlins	9	15	0.9386	1.9339	0.9326	2.3293	0.9315	2.3397
19	4-12-1	yes	MSE	tribas	satlins	8	10	0.9384	1.9381	0.9248	2.4560	0.9294	2.3718
20	4-23-1	yes	MSE	poslin	satlins	5	10	0.9389	1.9383	0.9451	2.1079	0.9417	2.1654

Code A.1 MATLAB code for estimation of the masonry wall compressive strength based on GEP model

```
clear; clc;
% Input
d(1) = input('Enter the value of the Masonry Unit Compressive Strength
(MPa)  :');
d(2) = input('Enter the value of the Mortar Compressive Strength
(MPa)  :');
d(3) = input('Enter the value of the Mortar thickness to Masonry unit
thickness ratio  :');

% Computing of the value of Masonry Prism Compressive Strength

G1C2 = -3.69857375928129;   G1C3 = -4.45177027159265e-02;
G2C9 = -15.8343505505162;   G2C6 = -4.89207688284471;
G2C0 = 3.03812680741293;    G3C8 = 9.56580756727409;
G3C6 = 26.314588309691;     G4C6 = 0.385461839301458;
G4C2 = 10.5638768473138;    G5C1 = -4.64339121677297;
G5C6 = 18.8783164760921;

y = (G1C2-(G1C3*(gep3Rt(((d(2)^2)-d(1)))*gep3Rt((d(1)^2)))))+
    gep3Rt((G2C9+(G2C6-((1.0/((((d(2)*d(2))-G2C0)^2)))^2))))+
    ((gep3Rt(((d(1)+d(1))/d(3)))+d(3))-(1.0/(((d(2)-
    G3C8)*gep3Rt(G3C6)))))+ gep3Rt((d(3)/((d(3)+((G4C2-
    d(2))/d(1)))*gep3Rt((G4C6/d(1))))))+ gep3Rt((((d(1)-
    ((d(1)-G5C6)*d(3)))^2)+(1.0/(((G5C1+d(2))^2)))));

% Results

X = [' The value of masonry compressive strength is :',num2str(y)];
disp(X);

function result = gep3Rt(x)
if (x < 0.0),
   result = -((-x)^(1.0/3.0));
else
   result = x^(1.0/3.0);
 end
```

Appendix B

In the following formulas, the obtained matrices that are required in the mathematical expression of the optimum ANN model, given by Equation 39, are presented.

Specifically, $[I_W]$ is given as:

$$[I_W] = \begin{bmatrix} -5.3910 & 1.5310 & -5.6512 \\ 9.3528 & -18.4219 & -6.0231 \\ 2.0582 & 14.0461 & 2.9575 \\ 5.1694 & 10.0439 & 12.7909 \\ -18.5102 & 16.7774 & 6.0558 \\ 0.3807 & -3.0667 & 0.7209 \\ 13.3363 & 0.0954 & 8.0548 \\ -7.3981 & -1.7045 & -18.4896 \\ -4.2164 & 4.8989 & -4.1091 \\ -3.2744 & 13.8312 & 13.8448 \\ -1.2817 & 4.0998 & -12.3361 \\ -0.6244 & 3.2565 & -1.0145 \\ -9.7726 & -34.8139 & -14.8376 \\ 5.7715 & -8.4101 & -16.3449 \\ -0.9708 & -0.6121 & 0.4154 \\ 3.2055 & -0.6710 & 7.6088 \\ -4.4868 & 0.2041 & 0.4323 \end{bmatrix} \quad (40)$$

while $[L_W]$, $[b_i]$ and $[b_0]$ are given by:

$$[L_W]^T = \begin{bmatrix} -1.5677 \\ 0.0227 \\ -0.3286 \\ -0.5525 \\ -0.9092 \\ -2.0052 \\ 1.0294 \\ 0.6070 \\ 0.4631 \\ -0.2270 \\ -0.6366 \\ 0.3000 \\ -0.1892 \\ 0.3112 \\ 1.3308 \\ 0.3252 \\ -1.9442 \end{bmatrix} \quad [b_i] = \begin{bmatrix} -13.3026 \\ 9.8899 \\ -6.7016 \\ -13.1773 \\ 6.1248 \\ 5.0079 \\ -5.4187 \\ 4.6020 \\ -0.2131 \\ -5.0976 \\ 0.0174 \\ 0.1619 \\ -3.9587 \\ 9.2426 \\ 0.8441 \\ 4.4998 \\ -4.9953 \end{bmatrix} \quad [b_0] = [-1.0581] \tag{41}$$

The $[IP]$ vector of the Input Parameters is given by

$$[IP] = \begin{bmatrix} 2\dfrac{f_{bc} - minf_{bc}}{maxf_{bc} - minf_{bc}} - 1 \\ 2\dfrac{f_{mc} - minf_{mc}}{maxf_{mc} - minf_{mc}} - 1 \\ 2\dfrac{t_m/\mathrm{t}_b - min(t_m/\mathrm{t}_b)}{max(t_m/\mathrm{t}_b) - min(t_m/\mathrm{t}_b)} - 1 \end{bmatrix} \tag{42}$$

where the min and max values of f_{wc}, f_{bc}, f_{mc} and t_m/t_b are given in Table 4.

References

ACI/TMS 122R-14, Guide to Thermal Properties of Concrete and Masonry Systems, Reported by ACI/TMS Committee 122, December 2014.

ACI 530.1-02/ASCE 6-02/TMS 602-02, Specification for Masonry Structures, Reported by the Masonry Standards Joint Committee (MSJC).

Alavi, A.H., Gandomi, A.H. (2012), Energy-based numerical models for assessment of soil liquefaction, Geoscience Frontiers, 3(4), 541-555.

Anthimopoulos, M., Christodoulidis, S., Ebner, L., Christe, A., Mougiakakou, S. (2016). Lung Pattern Classification for Interstitial Lung Diseases Using a Deep Convolutional Neural Network, IEEE Transactions on Medical Imaging, 35(5),7422082, pp. 1207-1216.

Apolo, G.L., Matinez-Luengas, A.L. (1995). Curso Técnicas de Intervención en El Patrimonio Arquitectonico, Consultores Tecnicos de Contstruccion, 1995.

Apostolopoulou, M., Douvika, M.G., Kanellopoulos, I.N., Moropoulou, A., Asteris, P.G. (2018), "Prediction of Compressive Strength of Mortars using Artificial Neural Networks", 1st International Conference TMM_CH, Transdisciplinary Multispectral Modelling and Cooperation for the Preservation of Cultural Heritage", Athens, Greece, 10-13 October.

Apostolopoulou, M., Armaghani, D.J., Bakolas, A., Douvika, M.G., Moropoulou, A., Asteris, P.G. (2019). Compressive strength of natural hydraulic lime mortars using soft computing techniques, Procedia Structural Integrity 17, 914–923.

Apostolopoulou, M., Asteris, P.G., Armaghani, D.J., Douvika, M.G., Lourenço, P.B., Cavaleri, L., Bakolas, A., Moropoulou, A. (2020). Mapping and holistic design of natural hydraulic lime mortars, Cement and Concrete Research, 136, 106167, https://doi.org/10.1016/j.cemconres.2020.106167

Armaghani DJ, Hajihassani M, Sohaei H, Mohamad ET, Marto A, Motaghedi H, Moghaddam MR (2015) Neuro-fuzzy technique to predict air-overpressure induced by blasting. Arab J Geosci 8(12):10937–10950.

Armaghani, D.J., Hatzigeorgiou, G.D., Karamani, Ch., Skentou, A., Zoumpoulaki, I., Asteris, P.G. (2019). Soft computing-based techniques for concrete beams shear strength, Procedia Structural Integrity 17 (2019) 924–933.

Armaghani, D.J., Asteris, P.G. (2020). A comparative study of ANN and ANFIS models for the prediction of cement-based mortar materials compressive strength, Neural Computing and Applications, 33, 4501–4532, https://doi.org/10.1007/s00521-020-05244-4

AS Committee 3700-2001. Masonry structures. Australian Standard Association, Sydney; 2001. 197pp.

Asteris, P.G., Antoniou, S.T., Sophianopoulos, D.S., Chrysostomou, C.Z. Mathematical macromodeling of infilled frames: State of the art, Journal of Structural Engineering, 2011, 137(12), 1508-1517.

Asteris, P.G., Cotsovos, D.M., Chrysostomou, C.Z., Mohebkhah, A., Al-Chaar, G.K. Mathematical micromodeling of infilled frames: State of the art, Engineering Structures, 2013, 56, 1905-1921.

Asteris, P.G., Plevris, V. (2013), "Neural network approximation of the masonry failure under biaxial compressive stress", Proceedings of the 3rd South-East European Conference on Computational Mechanics (SEECCM III), an ECCOMAS and IACM Special Interest Conference, Kos Island, Greece, June; pp. 584–598.

Asteris, P.G., Chronopoulos, M.P., Chrysostomou, C.Z., Varum, H., Plevris, V., Kyria-kides, N., Silva, V. Seismic vulnerability assessment of historical masonry structural systems, Engineering Structures, 2014, 62-63, 118-134.

Asteris, P.G., Plevris, V. (2016), "Anisotropic Masonry Failure Criterion Using Artificial Neural Networks", Neural Comput. Appl., 1–23, doi:10.1007/s00521-016-2181-3.

Asteris, P.G., Roussis, P.C., Douvika, M.G. (2017), "Feed-forward neural network prediction of the mechanical properties of sandcrete materials", Sensors (Switzerland), 17(6), 1344.

Asteris, P.G.; Argyropoulos, I.; Cavaleri, L.; Rodrigues, H.; Varum, H.; Thomas, J.; Lourenço, P.B. (2018). Masonry Compressive Strength Prediction using Artificial Neural Networks. In Proceedings of the International Conference on Transdisciplinary Multispectral Modeling and Cooperation for the Preservation of Cultural Heritage, Athens, Greece, 10–13 October 2018; Springer: Cham, Switzerland, 2018; pp. 200–224.

Asteris, P.G., Nozhati, S., Nikoo, M., Cavaleri, L., Nikoo, M. (2019), Krill herd algorithm-based neural network in structural seismic reliability evaluation, Mechanics of Advanced Materials and Structures, 26(13), 1146-1153.

Asteris, P.G.; Argyropoulos, I.; Cavaleri, L.; Rodrigues, H.; Varum, H.; Thomas, J.; Lourenço, P.B. (2018). Masonry Compressive Strength Prediction using Artificial Neural Networks. In Proceedings of the International Conference on Transdisciplinary Multispectral Modeling and Cooperation for the Preservation of Cultural Heritage, Athens, Greece, 10–13 October 2018; Springer: Cham, Switzerland, 2018; pp. 200–224.

Asteris, P.G., Mokos, V.G. (2019). Concrete Compressive Strength using Artificial Neural Networks, Neural Computing and Applications, https://doi.org/10.1007/s00521-019-04663-2.

Asteris, P.G., Douvika, M.G., Karamani, C.A., Skentou, A.D., Chlichlia, K., Cavaleri, L., Daras, T., Armaghani, D.J., Zaoutis, T.E. (2020). A Novel Heuristic Algorithm for the Modeling and Risk Assessment of the COVID-19 Pandemic Phenomenon, Computer Modeling in Engineering & Sciences, 125(2), 815-828, DOI:10.32604/cmes.2020.013280.

Asteris, P.G., Lemonis, M.E., Nguyen, T.A., Van Le, H., and Pham, B.T. (2021). "Soft computing-based estimation of ultimate axial load of rectangular concrete-filled steel tubes. Steel and Composite Structures, 39(4), 471.

ASTM C1314-18, Standard Test Method for Compressive Strength of Masonry Prisms, ASTM International, West Conshohocken, PA, 2018, www.astm.org.

Balasubramanian, S.R., Maheswari, D., Cynthia A., Rao, K.B., Prasad, M.A., Goswami, R., Sivakumar P. (2015). Experimental determination of statistical parameters associated with uniaxial compression behaviour of brick masonry, Current Science, 109(11), pp. 2094–2102.

Basha S. H. and Kaushik H. B., 2015. Evaluation of Nonlinear Material Properties of Fly Ash Brick Masonry under Compression and Shear, Journal of Materials in Civil Engineering (ASCE), 27 (8), 04014227.

Barbosa C.S., Lourenço P.B., Hanai J.B., 2010. On the compressive strength prediction for concrete masonry prisms. Mater Struct 43, 331–344. https://doi.org/10.1617/s11527-009-9492-0

Bartlett, P.L., 1998. The sample complexity of pattern classification with neural networks: the size of the weights is more important than the size of the network. IEEE transactions on Information Theory, 44(2), pp.525-536.

Bennett, R., Boyd, K., Flanagan, R. (1997). Compressive properties of structural clay tile prisms, J. Struct. Eng. 123 (7) (1997) 920–926.

Bosiljkov V., 2000. Experimental and numerical research on the influence of the modified mortars on the mechanical properties of the brick masonry. PhD Thesis, Slovenia, University of Ljubljana.

Bröcker, O. (1963). Die auswertung von tragfähigkeitsversuchen an gemauerten wänden, Betonstein-Zeitung, 19–21.

Cascardi, A., Micelli, F., Aiello, M. A. (2016). Analytical model based on artificial neural network for masonry shear walls strengthened with FRM systems. Composites Part B: Engineering, 95, 252-263.

Carvalho M.A.B., 2015. Development and validation of a constructive solution in BTC, Master Thesis, UniMinho (in Portuguese).

Gandomi, A.H., Alavi, A.H. (2012). Krill herd: A new bio-inspired optimization algorithm, Communications in Nonlinear Science and Numerical Simulation, 2012, 17(12), pp. 4831–4845

Garzón-Roca, J., Marco, C.O., Adam, J.M. (2013). Estimation based on neural networks and fuzzy logic. Compressive strength of masonry made of clay bricks and cement mortar. Eng Struct 48:21–27.

Gavriilaki, E., Asteris, P.G., Touloumenidou, T., ..Kokoris, S., Anagnostopoulos, A. (2021). Genetic justification of severe COVID-19 using a rigorous algorithm, Clinical Immunology, 2021, 226, 108726

Cavaleri L., Di Trapani F., Macaluso G., Papia M, 2012. Attendibilità dei modelli per la valutazione dei moduli elastici delle murature suggeriti dalle norme tecniche. Ingegneria sismica, 29(1), 38-59.

Cavaleri L., Di Trapani F., 2014. Cyclic response of masonry infilled RC frames: Experimental results and simplified modeling. Soil Dynamics and Earthquake Engineering, 65, 224-242.

Cavaleri L., Papia M., Macaluso G., Di Trapani F., Colajanni P., 2014. Definition of diagonal Poisson's ratio and elastic modulus for infill masonry walls. Materials and Structures, 47(1-2), 239-262.

Cavaleri, L., Chatzarakis, G.E., Di Trapani, F.D., Douvika, M.G., Roinos, K., Vaxevanidis, N.M., Asteris, P.G. (2017), "Modeling of surface roughness in electro-discharge machining using artificial neural networks", Advances in Materials Research (South Korea), 6(2), 169-184.

Cavaleri, L., Asteris, P.G., Psyllaki, P.P., Douvika, M.G., Skentou, A.D., Vaxevanidis, N.M. (2019). Prediction of Surface Treatment Effects on the Tribological Performance of Tool Steels using Artificial Neural Networks, Appl. Sci., 9(14), 2788.

Ceroni F., Pecce, M., Sica, S., Garofano A., 2012. Assessment of Seis-mic Vulnerability of a Historical Masonry Building. Buildings 2012, 2, 332-358.

Chen, H., Asteris, P.G., Armaghani, D.J., Gordan, B. and Pham, B.T. (2019). Assessing dynamic conditions of the retaining wall using two hybrid intelligent models. Appl. Sci. 2019, 9, 1042.

Christy,C.F., Tensing, D., Shanthi, R. (2013). Experimental study on axial compressive strength and elastic modulus of the clay and fly ash brick masonry, J. Civ. Eng. Constr. Technol. 4 (4) (2013) 134–141.

Chrysostomou, C.Z., Asteris, P.G. On the in-plane properties and capacities of infilled frames, Engineering Structures, 2012, 41, 385-402.

CSA S304-14 (2014). Design of Masonry Structures, Canadian Standards Association, Mississauga, ON, Canada.

Das, S.K., Samui, P., Sabat, A.K. (2011). Application of artificial intelligence to maximum dry density and unconfined compressive strength of cement stabilized soil, Geotechnical and Geological Engineering, 29(3), 329-342.

Darwin C. (1859). On the Origin of Species

Dayaratnam, P. (1987). Brick and Reinforced Brick Structures, Oxford & IBH, 1987.

Drougkas A., Roca P., Molins C., 2016. Compressive strength and elasticity of pure lime mortar masonry. Mater Struct 49, 983–999. https://doi.org/10.1617/s11527-015-0553-2

Dymiotis, C., Gutlederer, B.M. (2002). Allowing for uncertainties in the modelling of masonry compressive strength, Constr. Build. Mater. 16 (2002) 443–452.

EN 1052-1: Methods of test for masonry - Part 1: Determination of compressive strength, (1998), European Committee for Standardization, Brussels.

EN 1996-1-1 (2005) Eurocode 6: Design of masonry structures-Part 1-1: General rules for reinforced and unreinforced masonry structures, European Committee for Standardization, Brussels.

Engesser, F. Über weitgespannte Wölbbrücken, Zeitschrift für Architekturs und Ingenieurwesen, 1907, 53, 403-440 (in German).

Fortes E., Parsekian G., Fonseca F. (2014). Relationship between the compressive strength of concrete masonry and the compressive strength of concrete masonry units, J. Mater. Civil. Eng., 27 (9).

Francis A.J., Horman C.B., and Jerems L.E. (1970). The effect of joint thickness and other factors on the compressive strength of brickwork, 2nd International brick masonry conference, Stoke-on-Trent, 31-37.

Furtado A, Rodrigues H, Arêde A, Varum H. (2016). Experimental evaluation of out-of-plane capacity of masonry infill walls, Engineering Structures; 111, 48-63.

Furtado, A., Rodrigues, H., Arêde, A. et al. (2020). Mechanical properties characterization of different types of masonry infill walls. Front. Struct. Civ. Eng. 14, 411–434.

Gal, Y., Ghahramani, Z. (2016). Dropout as a Bayesian approximation: representing model uncertainty in deep learning, Proceedings of the 33rd International Conference on Machine Learning, New York. JMLR Workshop and Conference Proceedings, vol. 48, pp. 1050-1059.

Gayed M., Korany Y., Sturgeon G. (2012). Examination of the prescribed concrete block masonry compressive strength in the Canadian masonry design standard, CSA S304. 1-04 15th International Brick and Block Masonry Conference, Florianopolis, Brazil, 2012.

Graus S., Vasconcelos G., Palha C. (2019). Experimental characterization of the deterioration of masonry materials due to wet and dry and salt crystallization cycles. In: Aguilar R., Torrealva D., Moreira S., Pando M.A., Ramos L.F. (eds) Structural Analysis of Historical Constructions. RILEM Bookseries, vol 18. Springer, Cham.

Gregoire, Y. (2007). Compressive strength of masonry according to Eurocode 6: A contribution to the study of the influence of shape factors, Masonry International, MI Journal Article, 20.

Gumaste, K.S., Rao, K.S.N., Reddy, B.V.V., Jagadish, K.S. (2007). Strength and elasticity of brick masonry prisms and wallettes under compression, Mater. Struct. 40 (2) (2007) 241–253.

Haach, V., Vasconcelos, G., Lourenço, P.B. (2010). Experimental analysis of reinforced concrete block masonry walls subjected to in-plane cyclic loading, Journal of Structural Engineering, 136 (4), 452-462.

Hajihassani, M., Abdullah, S. S., Asteris, P. G., Armaghani, D. J. (2019), "A gene expression programming model for predicting tunnel convergence", Applied Sciences, 9(21), 4650.

Hendry,A.W., Malek, M.H. (1986). Characteristic compressive strength of brickwork walls from collected test results, Mason. Int. 7 (1986) (1986) 15–24.

Hendry A.W. (1998) Masonry Materials in Compression. In: Structural Masonry. Palgrave, London. https://doi.org/10.1007/978-1-349-14827-1_2.

Hilsdorf, H.K. (1969). An investigation into the failure mechanism of brick masonry loaded in axial compression in designing, Engineering and Constructing with Masonry Products, Eds. F. B. Johnson, Houston, Texas, 34-41.

Holický, M., Retief, J. V., Sýkora, M. (2016). Assessment of model uncertainties for structural resistance. Probabilistic Engineering Mechanics, 45, 188-197.

Hornik, K., Stinchcombe, M., White, H. (1989), "Multilayer feedforward networks are universal approximators", Neural Networks, 2, 359-366.

Jiang, K., Han, Q., Bai, Y., Du, X. (2020). Data-driven ultimate conditions prediction and stress-strain model for FRP-confined concrete. Composite Structures, 242, 112094.

Khandelwal, M., Armaghani, D.J., Faradonbeh, R.S., Ranjith, P.G., Ghoraba, S. (2016). A new model based on gene expression programming to estimate air flow in a single rock joint. Environ Earth Sci 75(9):739-86.

Karlik, B. and Olgac, A.V. (2011). Performance analysis of various activation functions in generalized MLP architectures of neural networks. International Journal of Artificial Intelligence and Expert Systems, 1(4),111-122.

Kaushik, H.B., Rai, D.C., Jain, S.K. (2007). Stress-strain characteristics of clay brick masonry under uniaxial compression, Journal of Materials in Civil Engineering, 19(9), 728-739.

Kechagias, J., Tsiolikas, A., Asteris, P., Vaxevanidis, N. (2018). Optimizing ANN performance using DOE: Application on turning of a titanium alloy, MATEC Web of Conferences, 178, 01017.

Khan, A. and Lemmen, C. (2013). Bricks and urbanism in the Indus valley rise and decline. Am. J. Archaeol. Available online: http://arxiv.org/pdf/1303.1426.

Koza, J.R. (1992). Genetic programming: on the programming of computers by means of natural selection, MIT Press, Cambridge, MA, United States.

Kumavat, H.R. (2016). An experimental investigation of mechanical properties in clay brick masonry by partial replacement of fine aggregate with clay brick waste, J. Inst. Eng. India Ser. A 97 (3) (2016) 199–204.

Le, T.T., Asteris, P.G. and Lemonis, M.E. (2021). "Prediction of axial load capacity of rectangular concrete-filled steel tube columns using machine learning techniques", Engineering with Computers, in press.

Lourakis, M.I.A. (2005). A brief description of the Levenberg-Marquardt algorithm implemented by levmar, Hellas (FORTH), Institute of Computer Science Foundation for Research and Technology, http://www.ics.forth.gr/~lourakis/levmar/levmar.

Lourenço, P. (2002). Computations on historic masonry structures, Progress in Structural Engineering and Materials, 4 (3), 301-319.

Lourenço, P.B., Vasconcelos, G., Medeiros, P., Gouveia, J. (2010). Vertically perforated clay brick masonry for loadbearing and non-loadbearing masonry walls, Construction and Building Materials; 24 (11), 2317-2330.

Lourenço, P.B., Avila, L., Vasconcelos, G. et al. (2013). Experimental investigation on the seismic performance of masonry buildings using shaking table testing. Bull Earthquake Eng 11, 1157–1190.

Lumantarna, R., Biggs, D.T., Ingham, J.M. (2014). Uniaxial compressive strength andstiff ness of field-extracted andlaboratory-constructed masonry prisms,J. Mater.Civ. Eng. 26 (4) (2014) 567–575.

Machado, J., Lübeck, A., Mohamad, G., Fonseca, F., Santos Neto, A., (2019). Compressive strength of masonry prisms under compression according to Eurocode 6 - EN 1996-1-1 (2005), Proceedings of the 13th North American Masonry Conference, Salt Lake City.

Mann, W. (1982). Statistical evaluation of tests on masonry by potential functions, Proceedings of the Sixth International Brick Masonry Conference, Rome, Italy, May, 1982, pp. 86–98.

Mauro, A. (2008). Long term effects of masonry walls. MSc thesis, University of Roma, Italy.

Medeiros, P., Vasconcelos, G., Lourenço, P.B., Gouveia, J. (2013). Numerical modelling of non-confined and confined masonry walls, Construction and Building Materials; 41, 968-976.

Milani, G., Lourenço, P.B., Tralli, A. (2006). Homogenised limit analysis of masonry walls, Part I: Failure surfaces, Computers and Structures, 84 (3-4), 66-180.

Mishra, M., Bhatia, A.S., Maity, D. (2019). A comparative study of regression, neural network and neuro-fuzzy inference system for determining the compressive strength of brick–mortar masonry by fusing nondestructive testing data, Engineering with Computers.

Mishra, M., Bhatia, A.S., Maity, D. (2020). Predicting the compressive strength of unreinforced brick masonry using machine learning techniques validated on a case study

of a museum through nondestructive testing, Journal of Civil Structural Health Monitoring, 10(3), pp. 389-403.
Mishra, M., Bhatia, A.S., Maity, D. (2021). A comparative study of regression, neural network and neuro-fuzzy inference system for determining the compressive strength of brick–mortar masonry by fusing nondestructive testing data, Engineering with Computers, 2021, 37(1), pp. 77–91.
Momeni, E., Nazir, R., Armaghani, D.J., Maizir, H. (2015). Application of artificial neural network for predicting shaft and tip resistances of concrete piles. Earth Sci Res J 19(1):85–93 87.
Mohamad G. (1998). Comportamento mecanico na ruptura de prismas de blocos de concreto., Master Thesis, Univeridade Federal de Santa Catarina, Florianópolis
Mohamad, G., Lourenço, P.B., Roman, H.R. (2007). Mechanics of hollow concrete block masonry prisms under compression: Review and prospects, Cement and Concrete Composites; 29(3), 181-192.
Mohamad, G., Lourenço, P.B., Roman, H.R. (2011). Mechanical behavior of concrete block masonry - Influence of vertical joint, 2011, 11th NAMC, Mineapolis, USA. (electronic source).
Mohebkhah A., (2007). A nonlinear-seismic model for brick-masonry-infill panels with openings in steel frames, Ph.D. thesis. Tehran (Iran): Tarbiat Modares University.
MSJC (Masonry Standards Joint Committee) (TMS 402/ACI 530/ASCE 5 and TMS 602/ACI 530.1/ASCE 6), Building Code Requirements and Specification for Masonry Structures, 2013.
Muñoz R., Lourenço P., Moreira S. (2018). Experimental results on mechanical behaviour of metal anchors in historic stone masonry Construction and Building Materials 163, 643-655.
Nagarajan, S., Viswanathan, S., Ravi, V. (2014). Experimental approach to investigate the behaviour of brick masonry for different mortar ratios, Proceedings of the International Conference on Advances in Engineering and Technology, Singapore, March, 2014, pp. 586–592.
National Concrete Masonry Association (2012). Recalibration of the Unit Strength Method for Verifying Compliance with the Specified Compressive Strength of Concrete Masonry.
Nwofor, T.C. (2012). Experimental determination of the mechanical properties of clay brick masonry, Canadian Journal on Environmental, Construction and Civil Engineering, 3 (3).
Oliveira J.V. (2014). Mechanical behavior of compressed earth blocks stabilized with alkaline activation. Master Thesis, University of Minho (in Portuguese).
Padalu, P.K.V.R., Singh, Y., Das, S. (2018). Uni-axial monotonic compresssive properties of brick masonry in India, Procedings of the 10th International Masonry Conference (IMC), Paper ID: 639, 1st Edition, 1639-1655, July 9-11, Milan, Italy.
Radovanović, Ž., Sindjic-Grebovic, R., Dimovski, S., Serdar, N., Vatin, N., Murgul, V. (2015). Testing of the Mechanical Properties of Masonry Walls – Determination of Compressive Strength. Applied Mechanics and Materials. 725-726. 410-418.
Rahimi, I.; Gandomi, A.H.; Asteris, P.G.; Chen, F. Analysis and Prediction of COVID-19 Using SIR, SEIQR, and Machine Learning Models: Australia, Italy, and UK Cases. Information 2021, 12, 109. https://doi.org/10.3390/info12030109
Ramesh, A., Hajihassani, M., Rashiddel, A. (2020), Ground movements prediction in shield-driven tunnels using gene expression programming, The Open Construction & Building Technology Journal, 14(1).
Raposo P, Furtado A, Arêde A., Varum H. and Rodrigues H. (2018). Mechanical characterization of concrete block used on infill masonry panels. International Journal of Structural Integrity, 9 (3), 281-295.

Ravula, M.B., Subramaniam, K.V.L. (2017). Experimental investigation of compressive failure in masonry brick assemblages made with soft brick, Materials and Structures, 50(19), 1-11.
Reddy, B.V., Vyas, C.V.U. (2008). Influence of shear bond strength on compressive strength and stress-strain characteristics of masonry, Materials and Structures, 41 (10), 1697-1712.
Samui, P. (2008). Support vector machine applied to settlement of shallow foundations on cohesionless soils, Computers and Geotechnics, 35 (3), 419-427.
Samui, P., Kothari, D.P. (2011). Utilization of a least square support vector machine (LSSVM) for slope stability analysis, Scientia Iranica, 18(1), 53-58.
Sadowski, L., Nikoo, M. (2014). Corrosion current density prediction in reinforced concrete by imperialist competitive algorithm, Neural Computing and Applications, 25(7-8), 1627-1638.
Sandeep, M.V., Renukadevi, S., Manjunath, S. (2013). Behavior of hollow concrete block masonry prism under compression-An experimental and analytical approach, International Journal of Research in Engineering and Technology (electronic source).
Sarhat, S.R., Sherwood, E.G. (2014). The prediction of compressive strength of ungrouted hollow concrete block masonry, Construction and Building Materials, 58, 111-121
Shivaraj Kumar, H.Y., Renuka Devi, M.V., Sandeep, Manjunath, S., Somanath, M.B. (2014). Effect of prism height on strength of reinforced hollow concrete block masonry, International Journal of Research in Engineering and Technology; 03 (06) (electronic source).
Singh, S.B., Munjal, P. (2017). Bond strength and compressive stress-strain characteristics of brick masonry, Journal of Building Engineering, 9, 10-16.
Syrmakezis, C.A., Asteris, P.G. (2001) Masonry failure criterion under biaxial stress state, Journal of Materials in Civil Engineering, 13(1), 58-64.
Tassios T. P. (1986). Mechanics of masonry, NTUA: Athens (in greek and in italian).
Tassios, T.P. & Chronopoulos, M.P. (1986). “A seismic dimensioning of interventions (repairs/strengthening) on lowstrength masonry building”, Middle East and Mediterranean Regional Conference on Earthen and low-strength masonry buildings in seismic areas, Ankara, Aug.-Sept., 1986.
Tassios, T.P. (1988). Meccanica delle Murature. Liguori Editore, Napoli.
Thaickavil, N.N., Thomas, J. (2018). Behaviour and strength assessment of masonry prisms, Case Studies in Construction Materials, 8, 23-38.
Thamboo, J.A. Development of Thin Layer Mortared Concrete Masonry (Ph.D. Dissertation), Queensland University of Technology, Brisbane, 2014.
Thamboo, J. A., Dhanasekar, M. (2019). Correlation between the performance of solid masonry prisms and wallettes under compression, Journal of Building Engineering, 22, 429-438.
TMS 402 (2011). Building Code Requirements and Specification for Masonry Structures and Related Commentaries. American Concrete Institute, Farmington Hills, Michigan, 236 pp.
Vasconcelos, G., Lourenço, P.B. (2009). Experimental characterization of stone masonry in shear and compression. Construction and Building Materials, 23 (11), 3337-3345.
Vindhyashree, Rahamath, A., Kumar, W.P., Kumar, M.T. (2015). Numerical simulation of masonry prism test using ANSYS and ABAQUS, International Journal of Engineering Research and Technology, 4(7), 1019–1027.
Vyas, U., Reddy, V. (2010). Prediction of solid block masonry prism compressive strength using FE model. Mater Struct 43, 719–735. https://doi.org/10.1617/s11527-009-9524-9.
Wu, H-H., Wu, S. (2009). Various proofs of the Cauchy-Schwarz Inequality, Octogon Mathematical Magazine, 17(1), 221-229.

Wu, Y., Giger, M.L., Doi, K., Vyborny, C.J., Schmidt, R.A., Metz, C.E. (1993). Artificial neural networks in mammography: Application to decision making in the diagnosis of breast cancer, Radiology, 187(1), pp. 81-87

Xu, H., Zhou, J., Asteris, P.G., Armaghani, D.J., Tahir, M.Md. (2019). Supervised Machine Learning Techniques to the Prediction of Tunnel Boring Machine Penetration Rate, Appl. Sci., 9(18), 3715.

Zavalis R., Jonaitis B., Lourenço P. (2018). Experimental investigation of the bed joint influence on mechanical properties of hollow calcium silicate block masonry. Mater Struct 51, 85.

Zhou, Q., Wang, F., Zhu, F. (2016). Estimation of compressive strength of hollow concrete masonry prisms using artificial neural networks and adaptive neuro-fuzzy inference systems, Construction and Building Materials, 125, pp.199-204.